Geometries of doleritic intrusions in central Spitsbergen, Svalbard: an integrated study of an onshore-offshore magmatic province with implications for CO_2 sequestration

Kim Senger, Srikumar Roy, Alvar Braathen, Simon J. Buckley, Karoline Bælum, Laurent Gernigon, Rolf Mjelde, Riko Noormets, Kei Ogata, Snorre Olaussen, Sverre Planke, Bent Ole Ruud & Jan Tveranger

Senger, K., Roy, S., Braathen, A., Buckley, S.J., Bælum, K., Gernigon, L., Mjelde, R., Noormets, R., Ogata, K., Olaussen, S., Planke, S., Ruud, B.O. & Tveranger, J.: Geometries of doleritic intrusions in central Spitsbergen, Svalbard: an integrated study of an onshore-offshore magmatic province with implications for CO_2 sequestration. *Norwegian Journal of Geology,* Vol 93, pp. 143–166. Trondheim 2013, ISSN 029-196X.

Igneous intrusions emplaced during the Early Cretaceous are well exposed in central Spitsbergen within the Permian–Jurassic sedimentary succession. The doleritic intrusions are collectively classified as the Diabasodden Suite, and form part of the High Arctic Large Igneous Province. Though relatively easily accessible and very well exposed in places, the Diabasodden Suite dolerites remain underexplored and their prevalent geometry is particularly poorly understood. In this contribution we address this deficiency by mapping the distribution of the igneous complexes in both onshore and offshore areas of central Spitsbergen, using an integrated dataset incorporating 2D seismic data with magnetic profiles, high-resolution multibeam bathymetric data, digital elevation models, aerial photos, geological maps, a lidar model and fieldwork. The intrusions occur primarily as sills, typically less than 50 m thick but extending over 10 km laterally. Subordinate dykes, transgressive sill segments and saucer-shaped intrusions are also present. Increased structural complexity is evident in the higher parts of the stratigraphy, with sill/dyke interactions relatively common. Some exposed positive relief features on the seafloor are interpreted as resistant dolerite intrusions, based on bathymetric data, 2D seismic lines and magnetic profiles. An increased presence of pockmarks along the rims of these intrusions cropping out at the seafloor suggests a causal relationship between focused fluid flow and igneous intrusions. As well as describing the overall geometry of the igneous complex, we investigate the implications of igneous intrusions for fluid flow within a siliciclastic aquifer, highlighted by a study addressing potential subsurface CO_2 storage in central Spitsbergen. Fracture corridors along dykes suggest that fluid flow may be channelled along dykes across the stratigraphy, perhaps leaking into the lower part of the caprock. Furthermore, both enhanced flow along dykes and hampering of flow across dykes may affect the areal distribution of the CO_2 plume following injection of CO_2 into the affected aquifer.

Kim Senger, Centre for Integrated Petroleum Research (Uni CIPR), Uni Research, Allégaten 41, 5007 Bergen, Norway. Department of Arctic Geology, University Centre in Svalbard, P.O. Box 156, 9171 Longyearbyen, Norway. Department of Earth Science, University of Bergen, Allégaten 41, 5007 Bergen, Norway. Electromagnetic Geoservices AS, Dronning Mauds gt. 15, 0250 Oslo, Norway. Srikumar Roy, Department of Arctic Geology, University Centre in Svalbard, P.O. Box 156, 9171 Longyearbyen, Norway. Department of Earth Science, University of Bergen, Allégaten 41, 5007 Bergen, Norway. Alvar Braathen, Department of Arctic Geology, University Centre in Svalbard, P.O. Box 156, 9171 Longyearbyen, Norway. Present address: Department of Geosciences, University of Oslo, P.O. Box 1048, Blindern, 0316 Oslo, Norway. Simon J. Buckley, Centre for Integrated Petroleum Research (Uni CIPR), Uni Research, Allégaten 41, 5007 Bergen, Norway. Karoline Bælum, Department of Arctic Geology, University Centre in Svalbard, P.O. Box 156, 9171 Longyearbyen, Norway. Present address: Svalbard Science Forum, P.O. Box 506, 9171 Longyearbyen, Norway. Laurent Gernigon, Geological Survey of Norway, Leiv Eirikssons vei 39, 7040 Trondheim, Norway. Rolf Mjelde, Department of Earth Science, University of Bergen, Allégaten 41, 5007 Bergen, Norway. Riko Noormets, Department of Arctic Geology, University Centre in Svalbard, P.O. Box 156, 9171 Longyearbyen, Norway. Kei Ogata, Department of Arctic Geology, University Centre in Svalbard, P.O. Box 156, 9171 Longyearbyen, Norway. Present address: Dipartimento di Fisica e Scienze della Terra 'Macedonio Melloni', Università degli Studi di Parma, Campus Universitario – Parco Area delle Scienze 157/A, I–43124 Parma, Italy. Snorre Olaussen, Department of Arctic Geology, University Centre in Svalbard, P.O. Box 156, 9171 Longyearbyen, Norway. Sverre Planke, Volcanic Basin Petroleum Research AS, Oslo Innovation Center, Gaustadalléen 21, 0349 Oslo, Norway. Centre for Earth Evolution and Dynamics, University of Oslo, PO Box 1048, Blindern, 0316, Oslo, Norway. Bent Ole Ruud, Department of Earth Science, University of Bergen, Allégaten 41, 5007 Bergen, Norway. Jan Tveranger, Centre for Integrated Petroleum Research (Uni CIPR), Uni Research, Allégaten 41, 5007 Bergen, Norway.

E-mail corresponding author (Kim Senger): senger.kim@gmail.com

Introduction

Early Cretaceous igneous intrusions are common throughout the Arctic archipelago of Svalbard, and are well exposed in central Spitsbergen (e.g., Nejbert et al., 2011). The intrusions were synchronously emplaced along with geochemically similar magmatic rocks throughout the Arctic, classified as the High Arctic Large Igneous Province (HALIP; Maher, 2001). The HALIP event on

Svalbard occurred at *c.* 124.5 Ma (Corfu et al., 2013) and is thus significantly older than the well-known North Atlantic Igneous Province (53–70 Ma, e.g., Hansen et al., 2009 and references therein). On Svalbard, the dolerites are classified as the Diabasodden Suite (Dallmann et al., 1999). The intrusions have been investigated only in a limited number of studies, primarily concentrating on geological mapping and petrological descriptions (e.g., Tyrrell & Sandford, 1933; Birkenmajer & Morawski, 1960), geochemistry (e.g., Shipilov & Karyakin, 2010; Nejbert et al., 2011), palaeomagnetic studies (e.g., Jeleńska et al., 1978; Vincenz & Jeleńska, 1985) and K–Ar and Ar–Ar geochronology (e.g., Burov et al., 1977; Birkenmajer et al., 2010; Nejbert et al., 2011). The geometrical configuration of this onshore-offshore magmatic province, and more specifically how the intrusions affect the country rock at local and regional scale, is nonetheless poorly constrained.

An understanding of the geometry of an igneous system is important for a number of reasons; it is used to help constrain models for probable magma emplacement pathways by anisotropy of magnetic susceptibility (e.g., Airoldi et al., 2012), can help investigate geochemical variations within the magmatic system (e.g., Galerne et al., 2008), and reveal the relative chronology of igneous emplacement (e.g., Muirhead et al., 2012). It can also illustrate sill linkage mechanisms (e.g., Cartwright & Møller Hansen, 2006), characterise the impact on hydrocarbon prospectivity (e.g., Cukur et al., 2010), help in the detection of fractured igneous hydrocarbon reservoirs (e.g., Gudmundsson & Løtveit, 2012; Witte et al., 2012), assist in mapping sills and dykes that act as seals for hydrocarbons (Lee et al., 2006), help to understand the formation of closures in the overburden (e.g., Hansen & Cartwright, 2006), as well as provide input data for modelling the aureole contact processes and associated global climate change (e.g., Svensen et al., 2004; Aarnes et al., 2010). Furthermore, increased hydrocarbon exploration in sub-basalt provinces such as the Møre and Vøring basins offshore Norway and the Faroe–Shetland margin, with associated seismic imaging challenges (e.g., Gallagher & Dromgoole, 2008), serve as an incentive for studies of exposed igneous complexes which may be used as input for improved geophysical processing. With the availability of modern 3D seismic data, numerous authors have investigated the large- and medium-scale geometries of igneous systems (e.g., Thomson, 2004; Miles & Cartwright, 2010), but important subseismic (<10–50 m in dimension) features ultimately rely on fieldwork for their identification (e.g., Hansen et al., 2011).

Numerous studies addressing the geometry of igneous provinces have been published (e.g., Thomson & Hutton, 2004; Wetmore et al., 2009; Hansen et al., 2011). However, most work has focused on understanding igneous provinces by geophysical methods in areas of limited ground truth (e.g., Thomson, 2004; Minakov et al., 2012), or on field-based studies with limited regional-scale geophysical data (e.g., Hansen et al., 2011; Airoldi et al., 2012). Igneous intrusions, layer-transgressive dykes in particular, have also been shown, using numerical simulation (e.g., Morel & Wikramaratna, 1982), geophysical exploration methods (e.g., Chandra et al., 2006), hydrological well data (e.g., Chevallier et al., 2004; Perrin et al., 2011) and 3D seismic interpretation (Rateau et al., 2013), to affect fluid flow in volcanic basins. This dual nature of igneous intrusions acting both as barriers to and as carriers of fluid flow was recently shown by Rateau et al. (2013) to affect basin-wide hydrocarbon migration, but the migration pathways will always be related to the overall geometry of the igneous complex.

The Diabasodden Suite on Svalbard provides an opportunity to image a shallow magma plumbing system using both offshore and onshore data. Such outcrop-seismic correlation has recently proved successful when linking 'broken bridges' seen in subseismic outcrop scale and seismic data from the Faroe–Shetland margin (Schofield et al., 2012). Consequently, the Diabasodden Suite dolerites of Svalbard should be studied in more detail in order to constrain subseismic features of this onshore-offshore magmatic province. Understanding the regional geometry of the igneous bodies is also important for predicting fluid flow and is especially relevant for an ongoing CO_2 storage project in Longyearbyen. Planned injection into a Late Triassic–Mid Jurassic aquifer hosting Diabasodden Suite igneous intrusions (Braathen et al., 2012; Bælum et al., 2012) may result in injected fluids being channelled, hampered or compartmentalised by the intrusive units, depending on their geometry. No previous work has focused on the geometries of igneous intrusions on Spitsbergen, as attempted in the current study. While a saucer-shaped geometry has been proposed for Svalbard by Polteau et al. (2008), no details and locations were discussed. Furthermore, studies of the Svalbard dolerites have so far only focused either on the offshore (2D seismic; e.g., Digranes & Kristoffersen, 1995) or the onshore (fieldwork, sampling; e.g., Nejbert et al., 2011) components. Until now, the offshore-onshore linkage has been lacking.

In this paper, we present new and integrated data used to constrain the geometries of igneous intrusions in central Spitsbergen, Svalbard and discuss the implications of these intrusions for regional fluid flow. The main objectives of the study are: (1) to contribute to the general understanding of the Diabasodden Suite magma plumbing system; (2) to map possible saucer-shaped intrusions in central Spitsbergen; and (3) to discuss the possible implications of igneous intrusions on regional fluid flow and reservoir compartmentalisation related to potential CO_2 storage in the study area.

Geological setting

Svalbard represents an uplifted part of the Barents shelf and its well-exposed Proterozoic–Palaeogene succession

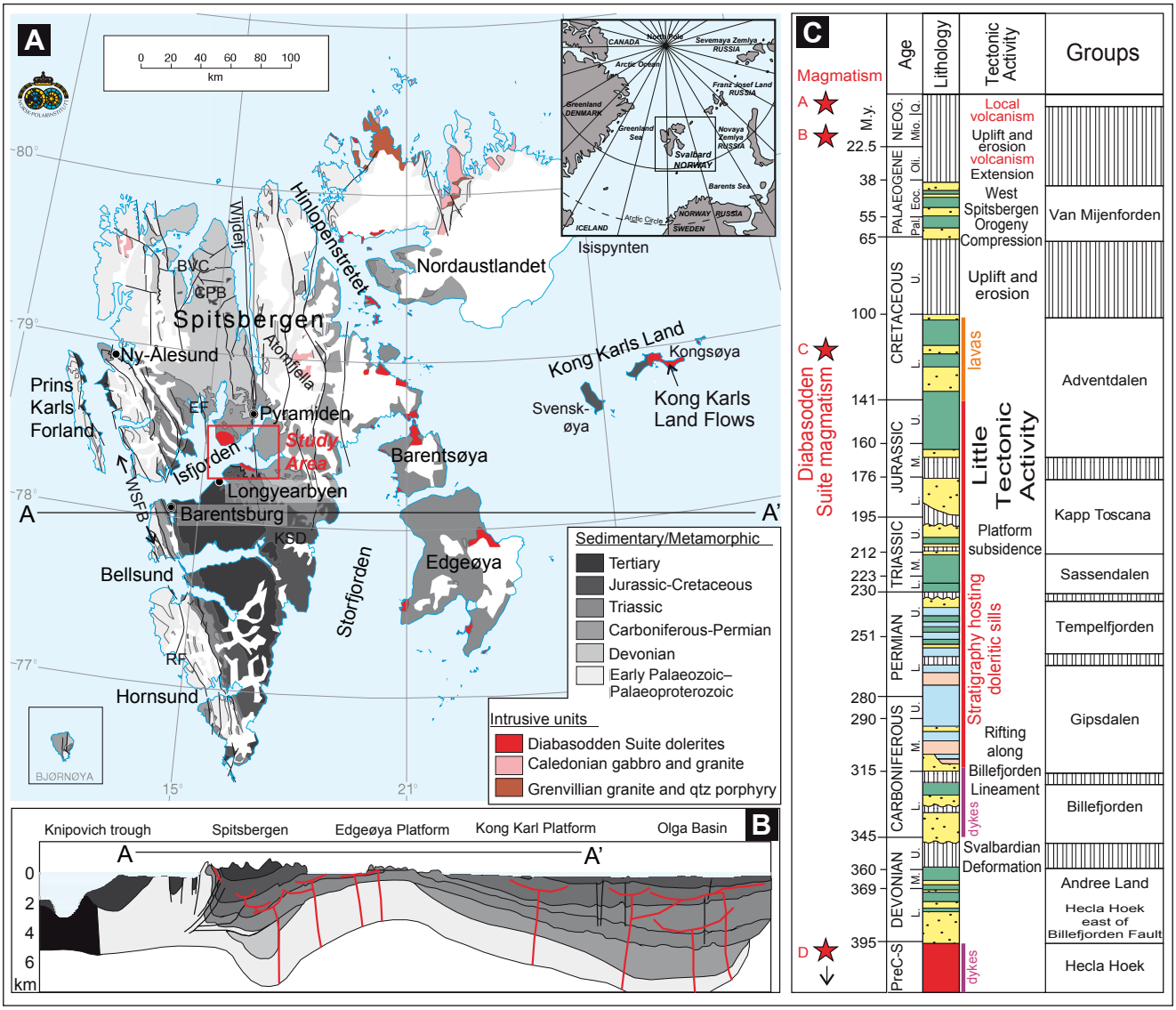

Figure 1. *Introduction to Svalbard geology. (A) Geological map of Svalbard, as modified from a Norwegian Polar Institute map (Elvevold et al., 2007). Spitsbergen is the largest island of the Svalbard archipelago and the study area in central Spitsbergen is marked with a red rectangle. Outcrops of Diabasodden Suite dolerites are highlighted in red. The inset map locates Svalbard in the context of the North Atlantic, approximately half-way between the North Pole and northern Norway. (B) Geological cross-section across Svalbard, highlighting the presence of the West Spitsbergen fold-and-thrust belt (WSFB) and associated foreland basin. Intrusions are represented schematically. A detailed map of the study area is shown in Fig. 3. The cross-section is based on an unpublished figure by Arild Andresen (University of Oslo). (C) Simplified stratigraphic column of Svalbard, adapted from Nøttvedt et al. (1993), illustrating the timing of Late Mesozoic magmatism and the intruded host rock units. The red stars A, B, C and D indicate the approximate timing of separate magmatic events on the archipelago, with the Early Cretaceous Diabasodden Suite highlighted. For a detailed stratigraphic column with formation names, refer to Fig. 14.*

(Fig. 1) serves as an analogue to the hydrocarbon provinces in the Barents Sea. The Svalbard archipelago consists of four main islands (Spitsbergen, Nordaustlandet, Edgeøya and Barentsøya) and numerous smaller islands scattered between 74–81°N and 10–35°E. The geological history of Svalbard has been reviewed by numerous authors (e.g., Steel & Worsley, 1984; Harland, 1997; Worsley, 2008) and is only briefly discussed here. Metamorphic basement rocks of the Hecla Hoek do not crop out in the study area, but are interpreted in 2D seismic data. A thick (up to 8 km) Devonian sedimentary package has been juxtaposed with the Hecla Hoek basement along the Billefjorden Fault Zone where a displacement of 6 km was interpreted in seismic data (Nøttvedt et al., 1993; Bælum & Braathen, 2012). This initially reverse fault, which strikes N–S across the study area, was reactivated as a normal fault during the Carboniferous, leading to the development of numerous half-grabens, as exemplified by the Billefjorden Trough located just north of the study area (e.g., Johannessen & Steel, 1992; Bælum & Braathen, 2012). In the Late Carboniferous, Svalbard evolved into a stable platform where sedimentation was primarily controlled by the northward drift. The majority of the host rocks to the igneous intrusions studied in central Spitsbergen was deposited during this phase. Due to the shift in latitude, sedimentation of Permian carbonates

shifted to siliciclastic-dominated deposition during the Mesozoic (Steel & Worsley, 1984; Blomeier et al., 2011). The Triassic is characterised by shale-siltstone-sandstone successions while the Jurassic to Early Cretaceous is represented by thick and homogeneous shales (e.g., Mørk et al., 1982; Høy & Lundschien, 2011). The platform cover deposits were intruded by the Diabasodden Suite dolerites during the Early Cretaceous (Maher, 2001; Nejbert et al., 2011), accompanied by regional uplift in northern Spitsbergen associated with the opening of the Amerasia Basin (Dörr et al., 2012). High-resolution U–Pb dating of rare pegmatite within the Diabasodden Suite suggests a main emplacement pulse at approximately 124.5 Ma (Corfu et al., 2013). In the study area, we used stratigraphic relationships, incorporating sequence thicknesses reported by Dallmann et al. (1999), to suggest that the magma was emplaced at a depth of at least 500 m. Farther east, on Kong Karls Land, time-equivalent lava flows are related to the same magmatic system (e.g., Smith et al., 1976).

Across the Arctic, time-equivalent magmatic units occur on Franz Jozef Land (e.g., Amundsen et al., 1998), Arctic Canada (e.g., Jackson & Halls, 1988), northern Greenland (e.g., Tegner et al., 2011) and the Siberian De Long Islands (e.g., Silantyev et al., 2004), and all are classified as part of the HALIP. Following Late Mesozoic intrusive activity, the Palaeogene oblique compression between Svalbard and Greenland led to the development of the West Spitsbergen fold-and-thrust belt (WSFB) and an associated foreland basin, the Palaeogene Central Spitsbergen Basin (e.g., Wennberg et al., 1994; Bergh et al., 1997; Helland-Hansen, 2010). The WSFB generated at least three eastward-extending thrust sheets soled in décollement zones along mechanically weak shale and evaporite layers (e.g., Bergh et al., 1997), identifiable on seismic profiles and in bathymetric data (Blinova et al., 2012). The thrust sheets probably separate the central Spitsbergen igneous complex from its feeder system. Palaeogene tectonics also reactivated the Billefjorden Fault Zone as a reverse fault uplifting the eastern hanging wall (e.g., Haremo et al., 1993). Finally, Quaternary unroofing associated with glacial activity has removed more than 1 km of Palaeogene and partly older sediments from the study area (Throndsen, 1982; Dimakis et al., 1998).

The 3500 km^2 extensive study area in central Spitsbergen occupies the northeastern edge of the Central Spitsbergen Basin where, due to a gentle regional dip (<3°), the Permian–Neogene sedimentary section is exposed (Figs. 2, 3). The seismic expression of the Central Spitsbergen Basin in the study area is described in recent contributions by Bælum & Braathen (2012) and Blinova et al. (2012). East of the Billefjorden Fault Zone, the study area is characterised by the Mesozoic platform deposits with several N–S-trending faults (Fig. 2).

Methods and data

Database

This study incorporates a range of pre-existing and acquired datasets (Table 1). Seismic, magnetic, lidar and borehole data have been integrated in the Petrel software (Schlumberger, 2011), together with topographic (digital elevation model, aerial photos, geological maps) and multibeam bathymetric data, summarised below into onshore and offshore data, respectively.

Onshore

Fieldwork was conducted within central Spitsbergen, primarily to characterise intrusion geometries. Fieldwork focused on the southern part of Dickson Land and the southern shore of Isfjorden between Flowerdalen and Deltaneset, with short campaigns studying the outcrops in inner Sassendalen. Geometries were mapped on the regional datasets, with field-based ground-truthing providing complementary measurements. The strike and dip of igneous bodies were measured using a GeoClino digital clinometer.

A digital elevation model (DEM) has been constructed for the entire study area from shapefiles with 20 m contour intervals, mapped at 1:100,000 scale by the Norwegian Polar Institute. The DEM was overlain with rasterised and vectorised geological maps from the NPI–Geonet project (NPI, 2011) and used to construct surfaces of igneous intrusion outcrops using Petrel. Dip azimuths and dip angles were then calculated for each grid cell. The DEM was complemented using high-resolution aerial photographs (pixel size 0.3–0.5 m) collected by the Norwegian Polar Institute. The individual images were georeferenced using ArcGIS and draped across the DEM to allow regional mapping of the intrusions.

A lidar ('Light detection and ranging') survey was acquired across the northern side of the Botneheia mountain by Helimap Systems AG in August 2009. The acquisition system integrated a laser scanner (Riegl LMS VQ–480, average point spacing of *c.* 0.5 m) to generate a point cloud, and a high-resolution digital camera (Hasselblad H3DII–50 50 MP digital camera with a 35 mm lens, pixel size 6.0 μm) to simultaneously acquire images for texturing the laser-generated topography. The system was mounted obliquely on a helicopter, allowing steep outcrop topography to be captured with optimum imaging geometry (Rittersbacher et al., 2013). Inertial and satellite positioning instruments recorded the trajectory of the data acquisition sensors, allowing the point cloud to be reconstructed during post processing. The point cloud and image data were processed according to Buckley et al. (2008). The result is a virtual outcrop model covering over 7 km of the cliff section at Botneheia. The setup gave an approximate image resolution of 0.07 m (with an average 400 m range), suitable for high-resolution mapping of both

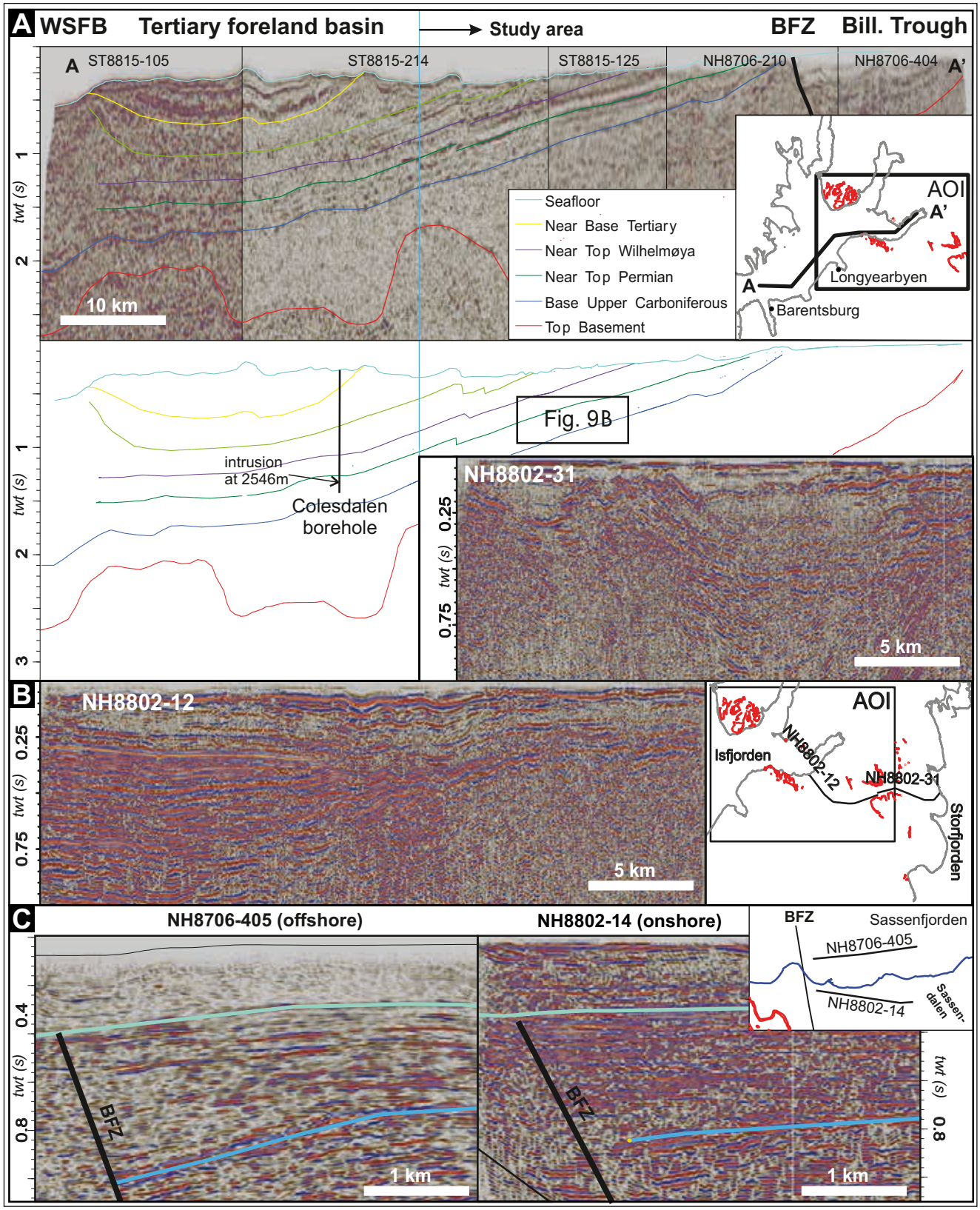

Figure 2. Seismic profiles introducing the study area. (A) Composite 2D seismic transect along Isfjorden illustrating the geological setting of the area of interest (AOI). The inset shows the location of the composite line, with the outcropping dolerites highlighted in red. (B) Regional seismic transect from Isfjorden to Storfjorden across the eastern segment of the study area. The onshore outcrops of the Diabasodden Suite are highlighted in red. (C) Onshore-offshore seismic line to illustrate the quality difference. The lines of comparable orientation illustrate the imaging of the Billefjorden Fault Zone (BFZ) and the associated syn-rift package. All vertical axes are shown in two-way-travel time in seconds. WSFB – West Spitsbergen Fold-and-thrust belt, BFZ – Billefjorden Fault Zone, Bill. Trough – Billefjorden Trough.

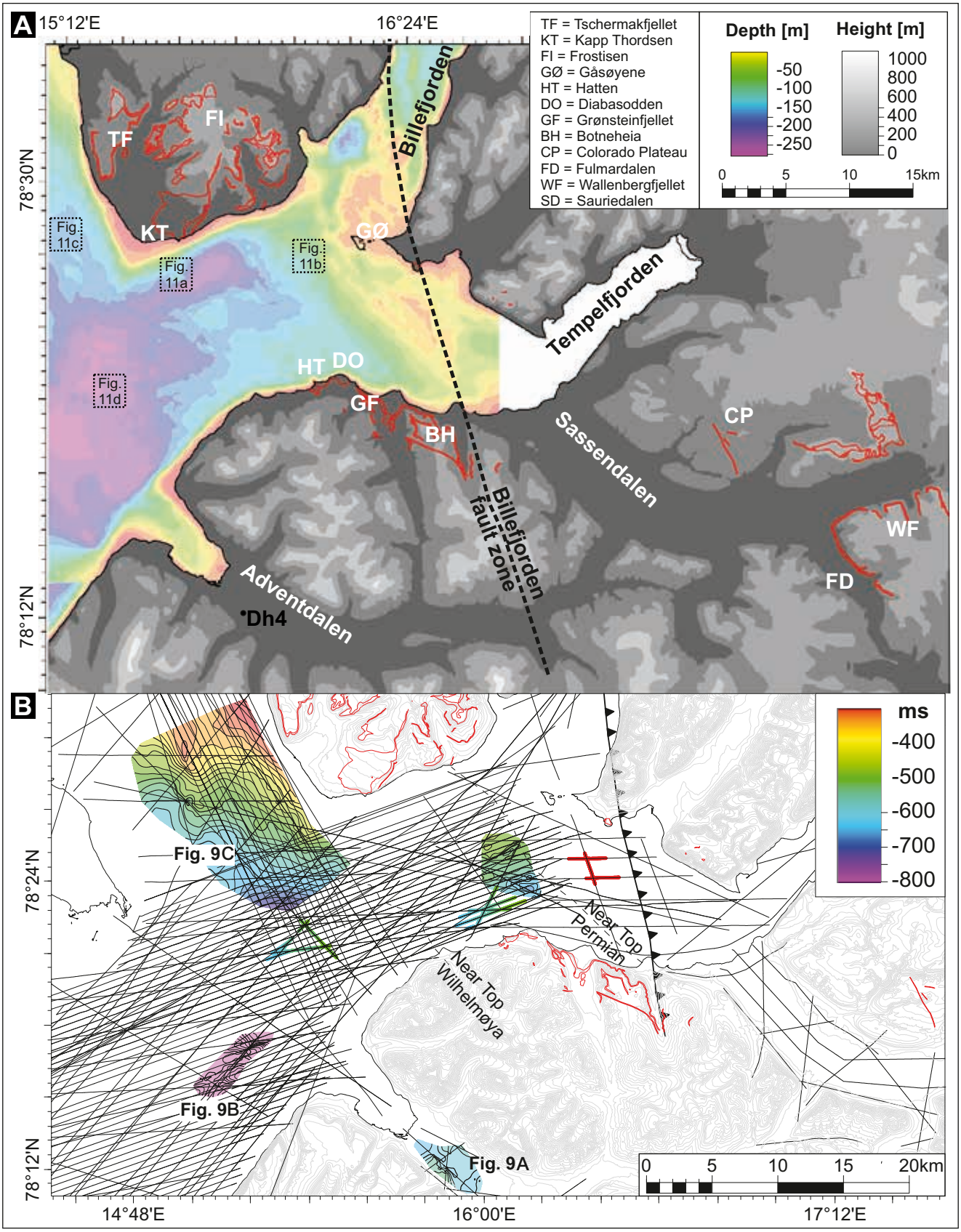

Figure 3. The study area location and database. (A) Detailed map of the inner Isfjorden study area, illustrating the outcropping dolerites (red), extent of bathymetric data, the drilled borehole Dh4 and the topography. The location of the bathymetric data illustrations presented in Fig. 11 is also shown. (B) Dolerite extent as mapped out using 2D seismic in inner Isfjorden. Where time-structure mapping is possible, the mapped extent of the interpreted intrusions is shown, with further detail in the corresponding Fig. 9. Additional reflectors tentatively interpreted as igneous intrusions but without sufficient data coverage to generate maps are illustrated as lines. The colour scale is in two-way-travel time (twt), and given in milliseconds. The available seismic database is shown as solid black lines, with thicker lines representing the Svalex 2D seismic profiles along which magnetic data was also acquired.

the dolerite and the host rock. Lidar data were interpreted using Petrel and in-house LIME software. Borehole data from Adventdalen, penetrating several thin sills, drilled by the Longyearbyen CO_2 project (Braathen et al., 2012), have been utilised to tie the target aquifer for CO_2 storage to the field area.

Offshore

High-resolution bathymetric data, acquired by the Norwegian Hydrographic Service using the Kongsberg EM1002 (95 kHz) and EM300 (30 kHz) multibeam echo sounders in 2008 and 2009, cover the entire study area. The multibeam bathymetric data were gridded with a 5 m horizontal cell size for visual examination of the seafloor and mapping of the various features and associated pockmarks.

The different physical properties of the igneous intrusions, particularly their high P-wave velocity of more than 6 km s^{-1} compared to the host rocks (3.5–4.5 km s^{-1}; Bælum & Braathen, 2012), allow their recognition and interpretation using seismic and magnetic data. The seismic database (Table 2, Fig. 3B) utilises existing commercial data acquired both onshore and offshore for hydrocarbon exploration in the 1980s (e.g., Eiken, 1994; Bælum & Braathen, 2012). Additional seismic data acquired onshore ties the CO_2 well park in Adventdalen to the regional seismic (Johansen et al., 2003), while 2D offshore data collected as part of the annual Svalex excursions cover large parts of inner Isfjorden (Asghar, 2011; Blinova et al., 2012). Onshore seismic data were acquired using the snowstreamer technology (e.g., Rygg et al., 1993) and is partly of comparable quality to the offshore data (Fig. 2C). Processing of the available seismic data typically focuses on removing the seafloor-multiple(s) related to the high velocities of the cemented bedrock at the seabed (Asghar, 2011) and the effect of onshore permafrost (Johansen et al., 2003). No additional seismic processing was undertaken in this study, but the colour table was optimised for visualising high amplitude reflectors.

The Svalex 2D offshore seismic data, shown in Fig. 3B, was complemented with magnetic data collected using a Geometrics G–882 caesium magnetometer, which has a ±10 nT precision and records every 10 seconds, subsequently resampled to 50 m spacing along the 2D seismic profiles. Preliminary magnetic processing involved residual spike removal, base station (located in Longyearbyen and Ny Ålesund) correction and calculation of the International Geomagnetic Reference Field (IGRF) for each profile. To correct the remaining diurnal magnetic variations, particularly important in this northern region (exceeding 150 nT), the magnetic dataset was levelled using a statistical method by which the discrepancies between the readings at each crossover point were reduced by systematically proportioning them between the tie (SSW) and line (NNW) profiles. The standard statistical levelling method used for this study involved fitting a low-order polynomial to the intersection errors by the method of least squares (e.g., Luyendyk, 1997; Mauring et al., 2002). These polynomials have then been subtracted from the original data, reducing the main intersection errors. After standard levelling, microlevelling

Table 1. *Summary of available datasets with corresponding coverage, resolution and usage.*

Data type	Coverage	Resolution (m)	Application	Data source
Topographic data	Whole study area	1:100,000	Generating DEM from contours, mapping	Norwegian Polar Institute
Airborne LiDAR (heli-based)	Botneheia	*c* 0.07 m	Interpretation of intrusions and sedimentology. Generate data on thickness	Acquired by UNIS CO_2 project
Digital elevation model (DEM)	Whole study area	20 m contours, mapped at 1:100,000	Mapping intrusions in 3D	Norwegian Polar Institute
DEM from LiDAR scan	Botneheia	2 m	Calculating intrusion thickness, mapping intrusions in relation to sediments	Acquired by UNIS CO_2 project
Aerial photos	Whole study area	*c* 1 m	Mapping intrusion extent	Norwegian Polar Institute
Seismic	Isfjorden, partly onshore in main valleys	10s of m	Mapping intrusion extent and form	Svalex, Statoil and Norsk Hydro
Multibeam bathymetric data	Isfjorden	5 m grid	Mapping pockmarks and seafloor morphology (e.g., resistant ridges)	Norwegian Hydrographic Survey
Magnetic data	Isfjorden, as Svalex 2D lines	Point every 50 m, line spacing *c* 500 m	Generating magnetic map of Isfjorden to identify magnetic anomalies	Svalex
Geological maps	Whole study area	1:100,000	Lineament analysis, outcrop extent calculation	Norwegian Polar Institute
Well data (drill cores, wireline logs)	Adventdalen	mm-scale (cores), dm-scale (wireline)	Dolerite sampling, fracture characterization	Drilled by UNIS CO_2 project
Fieldwork	Deltaneset, southern Dickson Land	N/A	Ground-truthing, fine-scaled mapping	New data

Table 2. *Overview of seismic lines used in this study. Only those lines intersecting the inner Isfjorden study area are tabulated. (irr) = irregular grid, typical line spacing is given where possible. Modified from Bælum & Braathen (2012).*

Survey	NH8509	ST8515	NH8706	ST8815	Svalex	NH8802	UNIS
Year	1985	1985	1987	1988	2001–2007	1988	2008–2011
Type	offhore	offhore	offshore	offshore	offhore	onshore	onshore
Purpose	commercial	commercial	commercial	commercial	academic	commercial	academic
Region	Isfjorden	Isfjorden, Billefjorden	Billefjorden, Tempelfjorden, inner Isfjorden	Isfjorden	Isfjorden	Nordenskiöld-land	Adventdalen
# of lines	14	13	19	23	55	26	7
Length (km)	244	262	271	270	713	237	18
Line spacing (km)	2	(irr)	(irr) 1.5	1.5–2.5	0.5	(irr) 1.5	(irr)
Source	airgun	airgun	airgun	airgun	airgun	dynamite	dynamite
Source specifics	2376 in^3	3781 in^3	3920 in^3	7840 in^3	1256–1406 in^3	Supercord	Dynacord, 0.4–4 kg per shot
Shot spacing (m)	25	25	12,5	25	50	50	10–50
Streamer length (m)	3000	2400	2000	3000	3000	1500	300–1500
# of groups	120	192	160	240	240	60	60
Group spacing (m)	25	12.5	12.5	12.5	12.5	25	5–25
Positioning system	GPS	SATNAV, GPS	Microfix	Microfix	GPS	n.a.	GPS

of the data has been carried out separately along the line and tie-line profiles, using a decorrugation technique (e.g., Ferraccioli et al., 1998; Geosoft, 2005). This technique is a frequency domain procedure based on a directional cosine filter combined with a Butterworth high-pass filter used to pass wavelengths on the order of two to four line separations. Such a process results from a preliminary line-to-line levelling error channel. Afterwards, a line-based low-pass filter was applied to this levelling error channel to separate the high-frequency geophysical signal from the longer wavelength levelling errors. The microlevelled channel result was finally obtained by subtracting the longer wavelength error channel from the original dataset and subsequently gridded using a minimum curvature gridding algorithm. The resulting magnetic map was draped on the bathymetric surface for interpretation.

Results

Igneous intrusions in the study area occur predominantly within the Triassic shale-sandstone sequence, cropping out in a 3 km (at Botneheia) to 12 km (beneath Frostisen) wide belt striking NW–SE, best illustrated in Fig. 3A. This belt continues to the northwest outside the study area, where dolerites are exposed around Dicksonfjorden (e.g., Vengeberget). Sills and dykes are also present in the Permian succession and commonly seen in evaporites and shales. Some dykes cut as high as the Lower–Middle Jurassic Wilhelmøya Subgroup, the upper part of the CO_2 storage aquifer. In 2D seismic, bathymetric and well data there are indications of igneous intrusion in the inner Isfjorden area, particularly in Sassenfjorden and parts of Nordfjorden. When mapped, they exhibit variable morphologies and geometries, as listed in Table 3.

Onshore

Fieldwork to map igneous outcrops was focused on the southern and northern shores of inner Isfjorden. Igneous intrusions are typically exposed as extensive (up to 10 km long) sills that commonly form the topographic tops of, for example, Sturefjellet and Kongressfjellet (Fig. 4B). Sills locally transgress across sedimentary layers, best exemplified at Tschermakfjellet (Fig. 4C). Subordinate dykes are present locally, and a likely feeder dyke is exposed at Rotundafjellet (Fig. 4E). The southern part of the study area, between Hatten and Flowerdalen, comprises younger siliciclastic rocks of the Tschermakfjellet, De Geerdalen and Knorringfjellet formations, overlain by the Agardhfjellet Formation shales. Igneous intrusions are typically more structured than in southern Dickson Land, comprising geometrically complex bodies of sills, transgressive sills and dykes, as exemplified by the Botneheia lidar model. Hatten may represent a stock through which the magmatic system was fed (Fig. 4A). A 30 m-thick regionally extensive sill extends across Botneheia towards Diabasodden. Structural measurements on Diabasodden suggest a curvature along a rim, which may be related to the inclined sheet of a saucer-shaped intrusion eroded to its present state.

The CO_2 target aquifer within the Kapp Toscana Group was mapped previously with respect to natural fracturing (Ogata et al., 2012). In the lower part of the target aquifer, the De Geerdalen Formation, numerous thick igneous intrusions are present at Diabasodden and Hatten (Fig. 4A). Thinner intrusions (c 2 m thick) are also present throughout the De Geerdalen Formation and the overlying Knorringfjellet Formation. One dyke, exposed at Botneheia, cuts through the Knorringfjellet Formation into the overlying shales of the Agardhfjellet Formation (part of the caprock succession for the CO_2 project).

Table 3. *Summary of characteristics of igneous features in inner Isfjorden, as illustrated through the various datasets.*

Data	Location	Dimensions			Comments
		Area	Length of intrusions	Height	
Geological maps	southern Dickson Land	140 km^2	up to 7 km continuous exposure	>100 m-thick sills (e.g., Rotundafjellet) in places, individual sills mostly < 50 m thick	Intrusions typically occur at tops of mountains (e.g., Rotundafjellet, Siklarhallet, Høyskolefjellet), some subordinate dykes present locally
	Diabas-Flowerdalen	29 km^2	>13 km continuous exposure	up to 160 m (Hatten, Diabasodden), mostly <50 m thick	Intrusions as complex network of sills and interconnected dykes (e.g., Grønsteinfjellet), thickest in the Hatten-Diabasodden area
	Rabotbreen	160 km^2	N/A	N/A	N/A
	Gipshuken	18 km^2	N/A	N/A	N/A
Seismic	offshore Bjørndalen	?	5 km	relief of c 130 ms (260 m)	Saucer-shaped geometry in 2D, occurs near Top Permian and may have some lift effect locally. Fault to the northeast. Occurs on strike to the CO_2 target aquifer.
	onshore Adventdalen	>19 km^2	min 7 km	up to 100 ms twt (200 m)	May consist of numerous stacked sills, masks Top Permian reflector, thin offshoot dykes are penetrated by DH4.
	north of Diabasodden, Permian section	up to 44 km^2	c 4.5 km	40 ms twt (80 m)	Follows stratigraphy, possible link to peculiar flat structure
	north of Diabasodden	N/A	3 - 5 km in diameter		Saucer-shaped morphology along one 2D line, no crossing tie lines. Sharp boundary between two saucers, high-amplitude reflection beneath the contact. Reminiscent of published saucers from Rockall Trough (Thomson, 2004).
	large dyke, north of Diabasodden	N/A	N/A	up to 700 ms deep (1400 m)	Seen by change in amplitude at four separate layers
Multibeam	Hatten dyke	N/A	1.2 km exposed offshore, up to 2.5 km if onshore continuation, branches into two onshore dykes	min. 120 ms twt, possibly up to 230 ms twt	Also visible on seismic section (ST8815–125), linked to high amplitude event
	Saucer-shaped intrusion	8.95 km^2	5.5 km long, 2.5 km wide	N/A	Elongated, resembles Karoo basin Golden Valley intrusion, occurs near Hatten dyke
	Hydrothermal vent complex or volcanic remnant	1.46 km^2	c 1.3 km radius	up to 90 m relief	c. 500 m diameter of inner part, positive relief feature, circular outer rim with 10–20 m relief, linking up with seismic ST8515–122
DEM	Wallenbergfjellet	N/A	7–10 km	30–50 m	Numerous offshoots, dipping into the mountain
	Tchermakfjellet	N/A	16 km exposure (circular)	N/A	One minor transgression, otherwise constant thickness following regional dip
	Sturefjellet	N/A	8.3 km circular exposure	N/A	Dolerite forms base for two lakes
	Skjørlokstupet	1.2 km^2	1.65 km long, 1.05 km wide	N/A	Elongated feature, very poorly exposed, partly covered by Grønsteinfjellet
LiDAR	Botneheia	N/A	8.3 km–long exposure scanned	variable	Multi-layer sills exposed

The exact point of penetration of the dyke into the Agardhfjellet Formation is unknown due to erosion, but intrusions (predominantly sills) within the Agardhfjellet Formation exposed on the east coast of Spitsbergen (Milovslavskij et al., 1993) indicate that the emplacement depth is shallowing eastwards, culminating in lava flows extruding on Kong Karls Land in the far east of the Svalbard archipelago.

The digital elevation model (DEM) allows the regional orientation of igneous intrusions to be visualised (Fig. 5). The study involved the comparison of two subsets; southern Dickson Land and the Diabas–Flowerdalen section along the southern shore of Isfjorden. It reveals an increased complexity in the southern section of the study area. On Dickson Land, sills are aligned with the regional stratigraphic dip with a dip azimuth of *c.* 190–220° and a dip of 3–13°. In contrast, the southern shore of Isfjorden is characterised by a complex intrusion geometry with an unclear directional component and a dip of 1–40°. The anomalous northerly dip azimuth may be an artefact of the north-facing topography of the study area. Aerial photos serve to illustrate the dolerite exposures in the study area with greater detail. Lineaments are particularly clear on the aerial photographs (Fig. 6). Structural measurements were taken at selected sites in order to ground-truth the

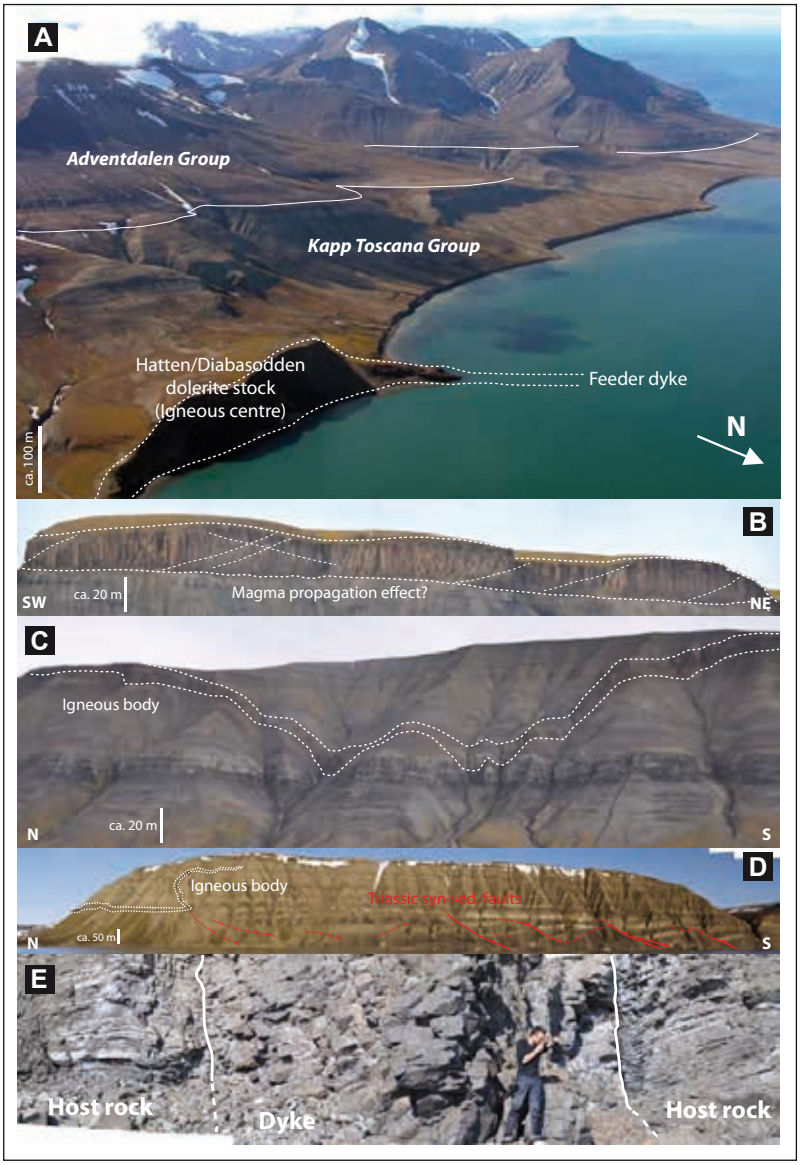

Figure 4. Examples of igneous features exposed in the study area. (A) Oblique aerial view of the Hatten igneous centre as well as the CO_2 storage aquifer within the Kapp Toscana Group. The top of the aquifer is marked by the white line, while the igneous centre is shown using stippled lines. Photograph by Winfried Dallmann (Norwegian Polar Institute). (B) Dolerite sill in Sauriedalen, southern Dickson Land. (C) Layer-transgressive sill exposed on the western slope of Tschermakfjellet. (D) Dolerite at Russebukta, Edgeøya, intruded along a fault in the Triassic sedimentary package. Photograph by Kei Ogata. (E) Dolerite dyke exposed on the beach beneath Rotundafjellet on the northern shore of Isfjorden. All photos by Kim Senger, except where noted.

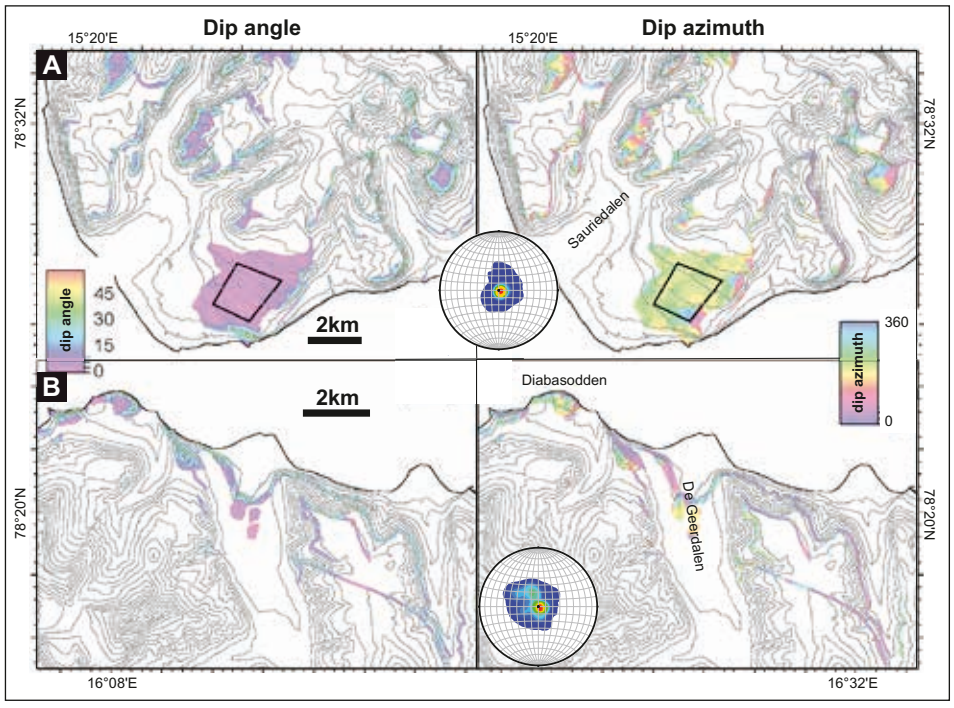

*Figure 5. Structural data on igneous intrusions derived from the digital elevation model in the study areas of the northern and southern shores of Isfjorden. The structural data are calculated at each grid cell (10*10 m grid cell size) and plotted using the colour scale for dip angle (left) and dip azimuth (right). The same data are also plotted as contoured stereoplots for the two areas, and illustrated in the inset stereoplots. (A) Dip angle (left) and dip azimuth (right) across southern Dickson Land. The Siklarhallet location is marked with a black rectangle. (B) Dip angle (left) and dip azimuth (right) across the southern shore of Isfjorden, between Flowerdalen and Diabasodden.*

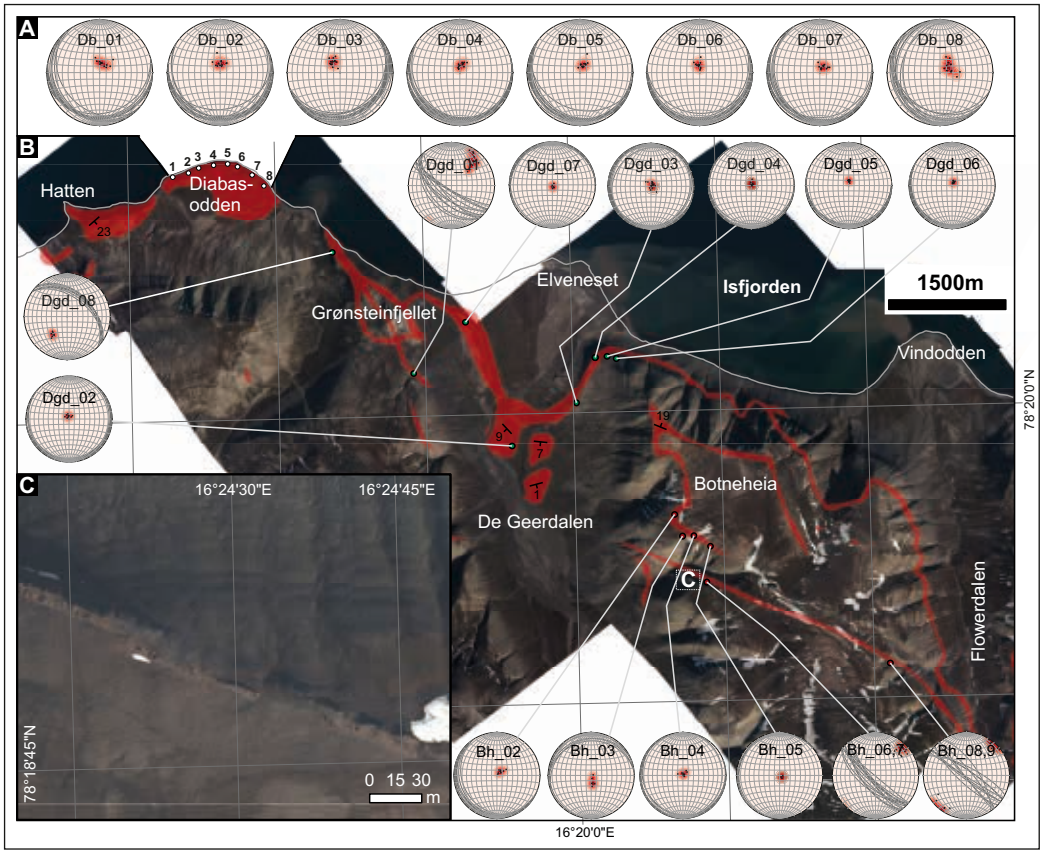

Figure 6. Aerial photo mosaic of the Diabasodden study area, illustrating the complex nature of the exposed dolerites and the field data on the dolerite orientation. (A) Stereoplots along the top of the Diabasodden rim suggest a possible saucer-shaped morphology of the rim, particularly for the easternmost structural stations Db–03 to Db–08. (B) Overview map of the whole study area, with structural stations from field (stereoplots) and 'virtual' structural stations derived from the DEM (strike/dip symbol). (C) Enlargement of the Botneheia dyke, illustrating its step-overs. The location of this dyke is highlighted with 'C' on the overview map. All stereoplots are contoured, with a lower-hemisphere, equal-area projection. Dolerite exposures, as mapped by NPI–Geonet, are shown in red. Aerial images provided by the Norwegian Polar Institute, batch number S2009–13835.

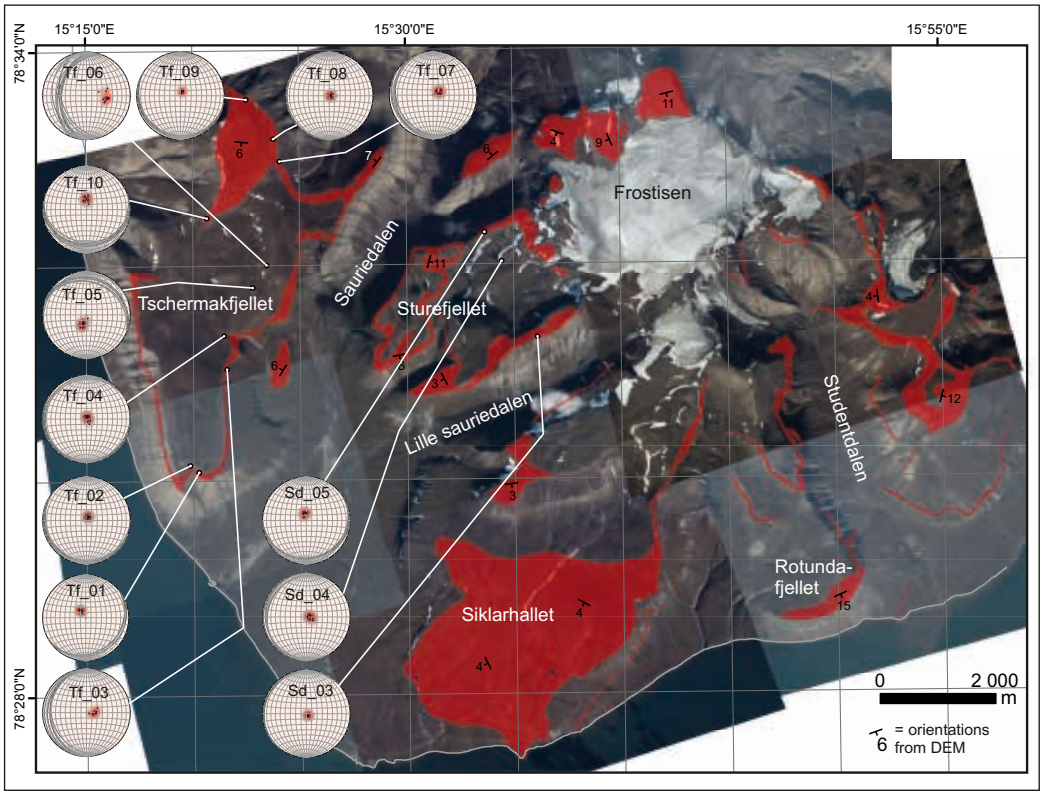

Figure 7. Aerial photograph mosaic of southern Dickson Land, illustrating structural data from fieldwork (stereoplots) and derived from DEM (strike/dip symbol). Note the predominance of generally layer-parallel sills forming the tops of mountains. All stereoplots are contoured, with a lower-hemisphere, equal-area projection. Dolerite exposures, as mapped by NPI–Geonet, are shown in red. Aerial photographs provided by the Norwegian Polar Institute, batch number S2011–25160.

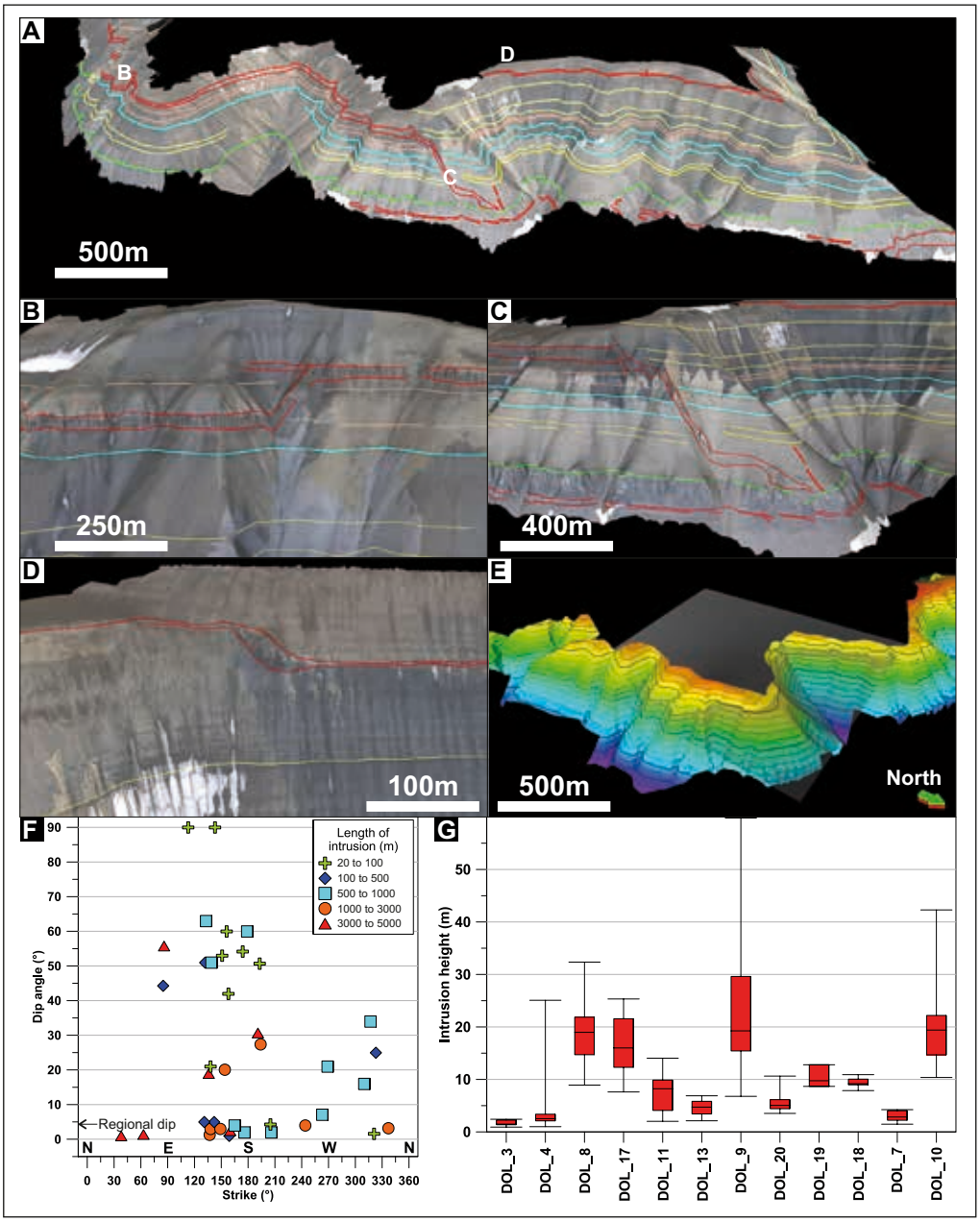

Figure 8. *Overview and details of igneous geometries from the lidar model of Botneheia. (A) The textured model of Botneheia allows for the interpretation of sedimentary units and igneous intrusions (red). The lettering corresponds to the enlarged images displayed in this figure. (B) An enlargement of a local sill transgression, with approximately 72 m offset between upper and lower parts. (C) A major transgressive system linking the upper and lower dolerite sills. (D) Thickening and merging of a thin sill. (E) Lidar point cloud imported into Petrel, with an example of a constructed top dolerite surface, shown transparent for clarity. (F) Strike and dip data derived from the lidar model, classified by intrusion length. Note particularly the short vertical dykes and a clustering of orientations along the regional dip. (G) Intrusion height data are derived from the lidar model and plotted as whisker plots with maximum, minimum and average, as well as upper and lower quartiles. All images are shown with a 3x vertical exaggeration.*

structural data from the digital elevation model (DEM). The measured orientations of the mapped exposures are illustrated in Figs. 6 & 7. The increased complexity on the south shore of Isfjorden is evident on the aerial mosaics, with one regional and extensive sill complemented by numerous inclined sheets and extensive dykes. On the northern side, sills are more regional in character and conform to the stratigraphy, transgressing only locally. Furthermore, numerous smaller-scale features are apparent on the high-resolution photographs. The dyke/sill interaction at Grønsteinfjellet (Fig. 6) is clearly visible in the aerial view. A well-exposed dyke at Botneheia, striking WNW–ESE, is exposed for more than 3 km, and illustrates step-over structures (Fig. 6C).

The lidar model of Botneheia documents intrusions at a very high resolution (Fig. 8). The textured surface is interpreted for both intrusions and sedimentary host rocks. Orientation data and geometrical data on the various intrusions were directly calculated from the virtual outcrop model (Fig. 8F, G). The intrusions appear to be striking predominantly N–S, though this may be biased due to the E–W orientation of the scanned and well-exposed Botneheia slope. Most intrusions (44%) dip at less than 10°, and line up with the regional dip of *c.* 3–5°. A cluster of intrusions (28%) transgress the host sediments, dipping between 40° and 60°, while only two (5%) short (<100 m) dykes are truly vertical. Orientations of the subvertical and vertical intrusions mapped on the lidar model line up with other mapped lineaments in the study area.

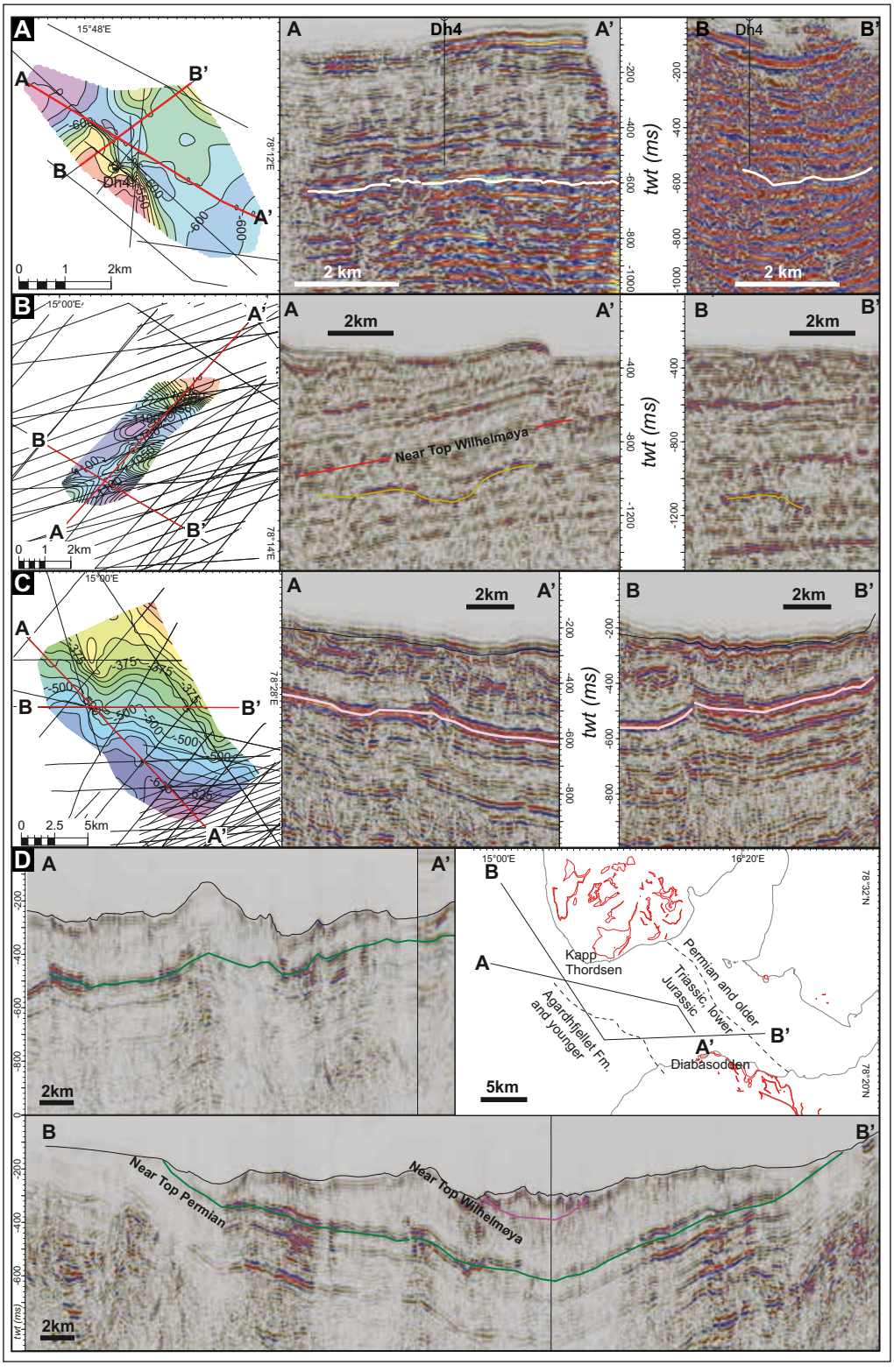

Figure 9. *Examples of igneous geometries on seismic sections throughout inner Isfjorden. For a location of the examples please refer to Fig. 3B. (A) High-amplitude reflectors located beneath the Dh4 borehole in Adventdalen. (B) A possible saucer-shaped intrusion offshore Bjørndalen. The likely intrusion occurs in the lower part of the CO_2 target aquifer. (C) Extensive, layer-parallel, high-amplitude reflection partially coincident with the Top Permian reflector, but possibly also locally enhanced by igneous intrusions. The intrusion has been previously interpreted by Digranes & Kristoffersen (1995). (D) Seismic correlation using two 2D composite lines across Isfjorden, linking the Kapp Thordsen and Diabasodden igneous centres.*

One borehole (Dh4) drilled by the Longyearbyen CO_2 laboratory project in Adventdalen penetrates one intrusion (2 m thick) at 950 m depth. This intrusion is analogous in size to intrusions exposed in the field around Hatten. Seismic data (Fig. 9A) suggest an intrusion of large enough dimensions to be identified on seismic data, probably thicker than *c.* 20 m, beneath the base of Dh4. Published literature confirms the presence of a 42 m-thick dolerite intrusion in a stratigraphic borehole drilled at Colesbukta, 20 km southwest of the study area (Skola et al., 1980).

Offshore

Igneous intrusions are interpreted using 2D seismic data throughout Isfjorden. A seismic tie from Kapp Thordsen to Diabasodden illustrates numerous high-amplitude reflectors within both Permian and Triassic host rocks (Fig. 9D). Furthermore, the composite sections highlight the absence of major faults between the two igneous centres, and it can therefore be assumed that the 'igneous belt' continues offshore across Isfjorden. It is possible to map out several reflectors interpreted to be sills or layer-transgressive sheets (Figs. 3B, 9). Igneous intrusions are interpreted on the basis of four characteristic features, as defined by Planke et al. (2005), and are particularly well-illustrated by one saucer-shaped reflector offshore Bjørndalen (Fig. 9B); (1) high amplitude, (2) locally transgressive, (3) abrupt terminations, and (4) saucer-shaped morphology.

A high-amplitude event is apparent in onshore seismic data *c.* 50 ms (equivalent to *c.* 100 m if a constant P-wave velocity of 4 km s^{-1} is assumed) beneath the base of DH4, as illustrated by Fig. 9A. This reflector is continuous for more than 7 km along a NW–SE trend and its extent is not fully constrained using the topography-controlled, onshore seismic database. Dh4 also penetrates a thin intrusion which may be an offshoot of a thicker intrusion below. A saucer-shaped reflector is evident offshore Bjørndalen and is shown in Fig. 9B. A high-amplitude

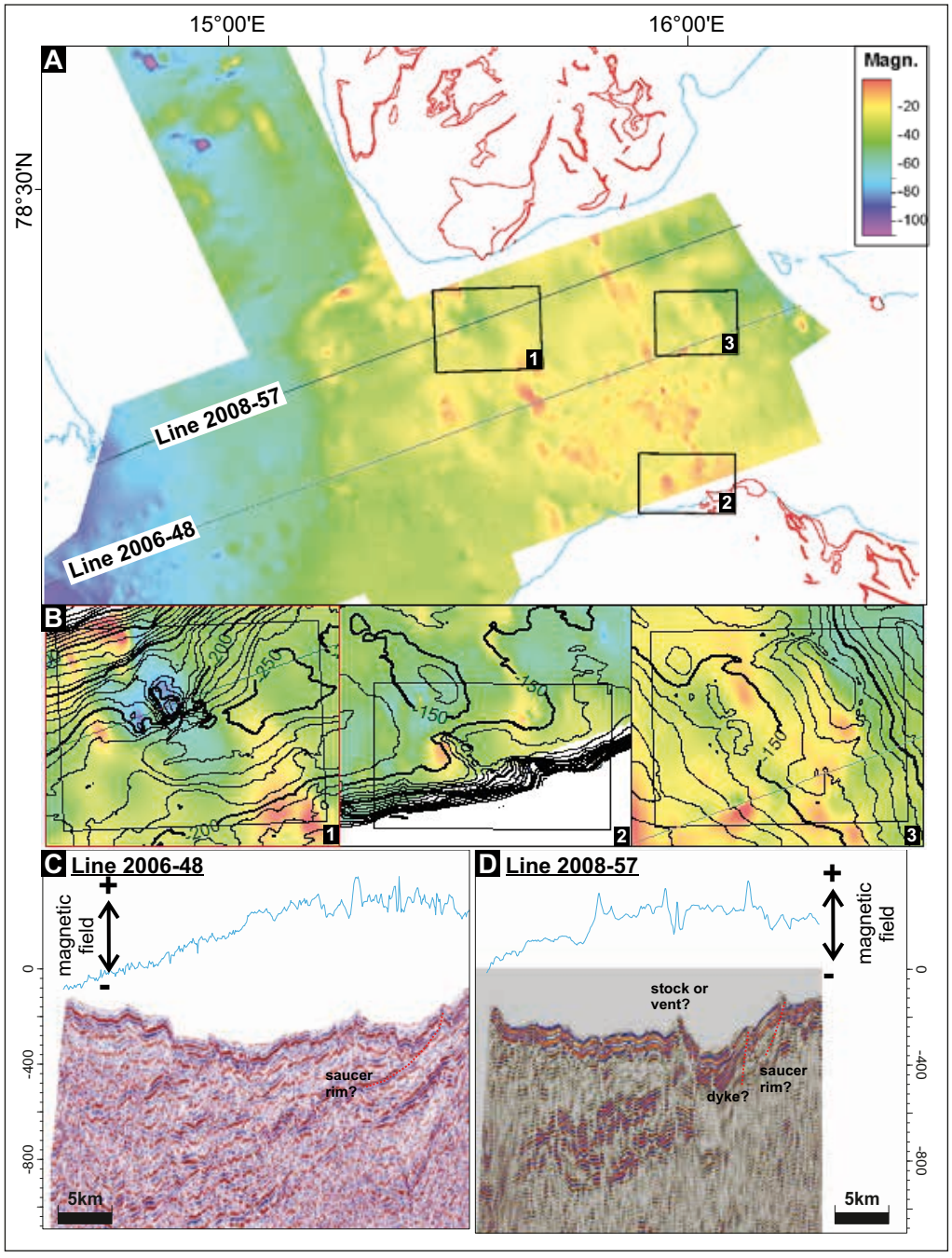

Figure 10. *Levelled total magnetic field anomalies from ship-based magnetic data, acquired by Svalex. (A) Overview map showing the interpolated magnetic map across the inner part of Isfjorden. The contours depict the water depth, and are contoured every 25 m. (B) Enlargements of selected areas of interest. Refer to overview map for location. 1 = residual magnetic low associated with a positive relief feature, interpreted as a possible hydrothermal vent complex. 2 = magnetic high associated with a positive relief feature extending from Hatten, interpreted as an offshore continuation of a doleritic dyke exposed on the surface. 3 = magnetic high beneath a curved positive relief feature, interpreted to be the inclined sheet of a saucer-shaped intrusion. (C) Magnetic profile (top) with corresponding 2D seismic profile (bottom) illustrating the possible outcropping rim of a saucer-shaped intrusion in Isfjorden. (D) Magnetic and seismic profile across a possible hydrothermal vent complex, suggested by the 'flowering' fault structure in the subsurface and the low-magnetic anomaly.*

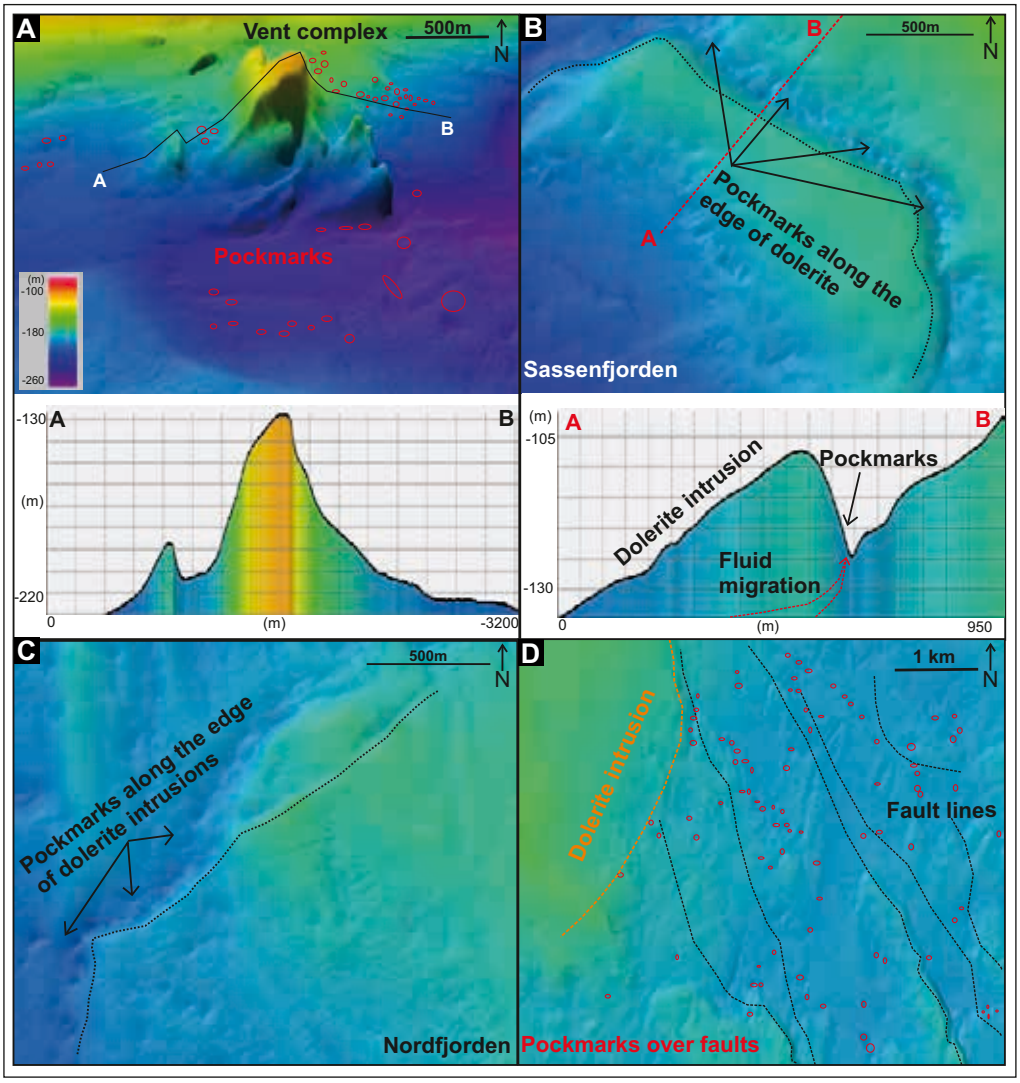

Figure 11. Examples of bathymetric expressions of dolerite intrusions, thrust faults and a possible hydrothermal vent complex, and their relationship to pockmarks. For locations of the examples refer to Fig. 3, and for details of the features and associated pockmarks please refer to Table 4. (A) Positive relief structure which may be interpreted as a hydrothermal vent complex, given the magnetic low anomaly depicted in Fig. 10. (B) Linear positioning of pockmarks along dolerite D3, indicating focused fluid flow along the base of the intrusions. (C) Pockmarks aligned along a probable intrusion in central Nordfjorden. (D) Regional bathymetric expressions of thrust faults interpreted by Blinova et al. (2012) and the scattered distribution of the associated pockmarks. Note particularly the focused distribution of pockmarks associated with dolerite intrusions, signifying efficient, directed and focused fluid flow along the intrusions.

reflector with abrupt terminations has been interpreted on the seismic, with the whole structure inclined to the regional dip. Two symmetric, layer-transgressive reflectors link an upper and a lower high-amplitude reflector. These are tentatively interpreted as the inclined sheets of a saucer-shaped intrusion, linking the inner and outer sills. A NW–SE–trending cross-line across the outer sill also displays abrupt terminations on both sides and minor layer transgression. A regionally extensive, high-amplitude reflection has been mapped southwest of Kapp Thordsen, as illustrated in Fig. 9C. This reflection has been previously interpreted as a dolerite intrusion by Digranes & Kristoffersen (1995). The reflection partly coincides with the regionally extensive and well-defined near Top Permian reflection, but is of exceptionally high amplitude in this area, with some minor structuration that could be caused by intrusion coalescence. Relatively thin, subvertical dykes are typically poorly imaged on seismic data, although they have been mapped in, for example, the Rockall Trough using 3D seismic data (e.g., Joppen & White, 1990; Thomson, 2004). In Isfjorden, 2D seismic data have been used in combination with bathymetric and outcrop data to delineate a *c.*100 m-wide doleritic dyke in the offshore-onshore transition zone near Hatten.

Overlaying the magnetic levelled total field on the bathymetric data reveals several strong anomalies within inner Isfjorden (Fig. 10). Linear magnetic highs striking NNW–SSE appear to link the southern and northern shores of Isfjorden, and may be related to a series of interconnected dykes and sills. Alternatively, they may be associated with thrust faults developing during the Palaeogene compression. Positive anomalies are also apparent in Nordfjorden, where a dolerite sill has been previously interpreted by Digranes & Kristoffersen (1995) and remapped in this study (Fig. 9C). While the actual sill lies at depth (approximately 700 m deep given an average P-wave velocity of 2.5 km s^{-1}) and appears flat on the seismic, the positive anomalies in Nordfjorden may represent a series of subseismic offshooting dykes or inclined sheets branching off from the main sill. A positive relief feature, also depicted in Fig. 11, clearly coincides with a residual magnetic low (Fig. 10B). A seismic profile across this feature (Fig. 10D) depicts its subsurface configuration,

with a flowering structure of complex faults. The feature is tentatively interpreted as a hydrothermal vent complex, and is discussed in detail below.

The high-resolution bathymetric coverage throughout Isfjorden allows for detailed interpretation of seafloor structures. Extensive glacial activity has carved out Isfjorden, and is manifested by iceberg plough marks, glacial lineations and recessional moraines (e.g., Baeten et al., 2010). The present-day morphology of the seafloor is characterised by numerous positive relief features, which have recently been interpreted as related to thrust tectonics associated with the West Spitsbergen fold-and-thrust belt (Blinova et al., 2012); ridges are competent rocks thrust over less competent units. High-magnetic anomalies associated with some sharp, curved, positive relief features in Sassenfjorden and Nordfjorden may alternatively be interpreted as exposed resistant dolerite ridges (Fig. 10). An extensive study of pockmarks in the study area has been undertaken by Roy et al. (2012). Their association with selected features is shown in Table 4 and Fig. 11. A distinct positive relief circular feature, 45–90 m high, is identified southeast of Kapp Thordsen (Fig. 11A). The feature consists of a main stock-like feature in the middle and an outer rim with inward-dipping surfaces. Some pockmarks are associated with the feature, but no clear pattern is evident. Magnetic data suggest a low-magnetic anomaly across the feature, and a 2D seismic profile illustrates the presence of a 'flowering' structure of faults (Fig. 10C). On this basis, and by analogue comparison with hydrothermal vent complexes in the Karoo Basin of South Africa (Svensen et al., 2006) and in the offshore Faroe–Shetland Basin (Grove, 2013), this feature is suggested to represent a hydrothermal vent complex formed during the explosive degassing following magma emplacement. Dolerite D3, with a corresponding magnetic high shown in Fig. 10B, has *c.* 24 pockmarks aligned along its northeastern margin. A similar intrusion, D4, has been identified in the centre of Nordfjorden, illustrated in Fig. 11C. The ridge has a relief of 8–10 m and may be related to a dyke branching off the high-amplitude seismic reflector shown in Fig. 9C. Pockmarks are clustered along the northwestern margin of this feature. Sharp positive relief features have been identified throughout inner Isfjorden, generally aligned N–S or NNW–SSE (Fig. 11D). These features have previously been interpreted as seafloor expressions of thrust faults (Blinova et al., 2012). Pockmarks are also associated with these features, but in contrast to the dolerite ridges the pockmarks tend to be more spread out and show only minor alignment. Aligned pockmark strings and high-density pockmarks associated with igneous intrusions may thus provide circumstantial evidence for enhanced fluid flow channelled around igneous intrusions.

Overall geometry

Based on the observed igneous geometries in the study area, it is possible to establish a series of profiles across the northern and southern study areas as shown in Fig. 12.

Table 4. *Summary of bathymetric features and associated pockmarks as identified on the multibeam bathymetric data.*

Feature								
Figure	Location and extent	Orientation	Water depth (m)	Relief (m)	Comment	Bedrock age	diameter (m)	depth (m)
Hydrothermal vent complex (Fig. 11a)	offhsore Kapp Thordsen	circular	200–220	45–90	The main stock is 45–90 m high in the middle with an inward-dipping outer rim. Pockmarks are randomly distributed all around the feature.	Triassic – Lower Jurassic	10–22	1–2
Dolerite D1 and D2	Billefjorden–Sassenfjorden intersection. is 12 km long, D2 is 15 km long.	NW–SE, dips SW	40–60	20–30	Cluster of c. 80–100 pockmarks aligned SW of the D2 sill, few pockmarks are located between D1 and D2.	Carboniferous – Permian	15–20	1–2
Dolerite D3 (Fig. 11B)	Mouth of Billefjorden. Divided into two parts – the NW section is 1.6 km and SW section is 2 km long.		120–125	10–15	c 24 pockmarks aligned along the rim of the intrusion		20–30	1–2
Dolerite D4 (Fig. 11C)	Central Nordfjorden (3.4 km long in NW–SE direction & 2.6 km wide in the E–W direction).	NW–SE, outcrops towards E and N, dips SW.	180–215	6–10	Pockmark strings in the troughs at the N edge of the dolerite		30–35	1–2
Thrust fault (Fig. 11D)	Inner Isfjorden	NNW–SSE	165–270	10–22	165 pockmarks located over the thrust faults, with no particular alignment	Triassic – Lower Jurassic	22–213	1–7

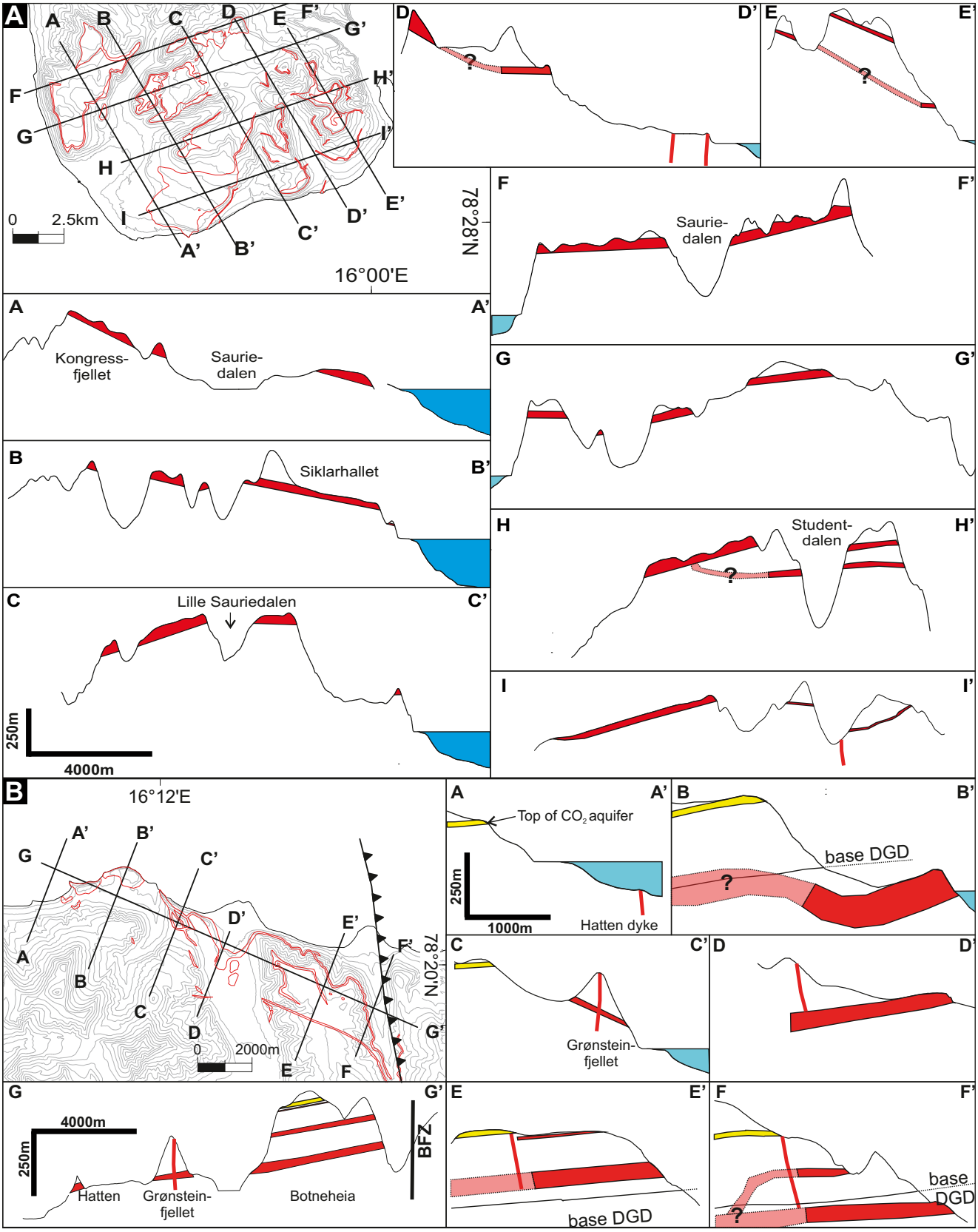

Figure 12. Cross-sections across the field area, illustrating the outcropping dolerites and possible subsurface configuration of the intrusions. (A) Profiles across southern Dickson Land, characterised by layer-parallel sills, in places stacked on top of each other. (B) Profiles across the Diabas–Flowerdalen section, characterised by increasingly complex geometries including a possible saucer-shaped intrusion at Diabasodden and numerous dykes. In the profiles the upper part of the CO_2 target aquifer, the Knorringfjellet Formation, is illustrated. An additional c. 250 stratigraphic metres beneath the Knorringfjellet Formation, namely the De Geerdalen Formation, is also considered as part of the aquifer. BFZ – Billefjorden Fault Zone, DGD – De Geerdalen Formation, Tmk. – Tschermakfjellet Formation, Btn. – Botneheia Formation, Vk. – Vikinghøgda Formation.

Sills are clearly the dominant and areally most extensive form of intrusion, particularly in southern Dickson Land. The main sill in De Geerdalen thins towards both the southeast and the northwest, and transgresses to a higher level in both directions. The presence of at least five dykes within the relatively narrow (1–5 km) exposure belt between Hatten and Flowerdalen implies a predominance of dykes in this stratigraphically shallower interval compared to the deeper part of the succession exposed on the northern shore of Isfjorden. This pattern could reflect the presence of a feeder stock south of Isfjorden, represented by Hatten.

Discussion

Evidence of saucer-shaped intrusions on Spitsbergen

Saucer-shaped intrusions have been identified in numerous sedimentary basins globally, including Senegal (e.g., Rocchi et al., 2007), the Rockall Trough (e.g., Thomson & Hutton, 2004), the Faroe islands (Hansen et al., 2011) and the Karoo Basin of South Africa (e.g., Chevallier & Woodford, 1999; Polteau et al., 2008). They have also been proposed to exist on Svalbard (Polteau et al., 2008), though with no specific details of their location or physical evidence from geophysical and geological data. The current study has identified one clear saucer-shaped morphology on seismic data offshore Bjørndalen (Fig. 9B), with additional indications of possible saucer rims exposed both offshore (Fig. 11) and onshore at Diabasodden (Fig. 7A). 3D seismic offshore and additional 2D seismic onshore would be required to delineate saucer-shaped intrusions in more detail. Apart from likely saucer-shaped intrusions, there will also be a variety of other igneous geometries present. Sills and dykes are the dominant geometrical expressions of igneous intrusions in the study area, but using the Karoo igneous province as an analogue (e.g., Chevallier & Woodford, 1999), a range of igneous geometries is to be expected. Some 'traditional' sills, particularly on the north shore of Isfjorden with its substantial glacial cover, may actually represent the inner or outer sills of a saucer-shaped intrusion. A full range of igneous geometries is thus to be expected on Spitsbergen, being controlled by the emplacement depth, magma properties, intrusion chronology as well as the host rock properties.

Climate change implications

Numerous authors have postulated a link between emplacement of large igneous provinces (LIPs) and global climate change (e.g., Svensen et al., 2004; Aarnes et al., 2010). The emplacement of the Diabasodden Suite is constrained by a limited number of U–Pb radiometric ages clustered at 124.5 Ma (Corfu et al., 2013). The emplacement of the Diabasodden Suite is constrained by a limited number of U-Pb radiometric ages of dolerites from central and western Spitsbergen, as well as a bentonite in the Dh3 borehole in Adventdalen (Corfu et al. 2013). This age is somewhat synchronous with the oceanic anoxic event 1 (OAE1), as demonstrated by isotope data from the Dh3 borehole (Polteau et al., 2011)". However, additional dating is required to constrain the duration of the Diabasodden Suite magmatic event. Linkage between climate change and igneous intrusions requires mechanisms to transport the excess natural gas generated by enhanced maturation near intrusions to the atmosphere. On Svalbard, the majority of the Diabasodden Suite is emplaced at more than 1 km depth with the exception of the Kong Karls Land lava flows in the far east of the archipelago. Hydrothermal vent complexes have recently been postulated as possible mechanisms of linking intrusions with the oceans and atmosphere (e.g., Jamtveit et al., 2004; Planke et al., 2005). On Svalbard, such vent complexes have not been mapped in the past. However, our study suggests that such a hydrothermal vent complex may be present offshore Kapp Thordsen (Fig. 11A).

Linking pockmarks to dolerites

Pockmarks in Isfjorden represent focused fluid seepage sites at the seafloor and their distribution can thus be used to infer regional fluid-flow patterns. 356 individual pockmarks were identified in the study area using multibeam bathymetric data, of which less than 20% appear to be particularly associated with dolerite intrusions. The majority (80%) of pockmarks in the study area are generally associated with thrust faults (Blinova et al., 2012), suggesting fluid flow along fault zones. The pockmarks associated with igneous intrusions nonetheless show a focused occurrence of the pockmarks aligned along the outcropping edge of the intrusion (Fig. 11B, C). On the contrary, the pockmarks lying over the thrust faults in inner Isfjorden are more sparsely distributed (Fig. 11D), indicating less focused fluid flow when compared to the pockmarks found along the dolerite intrusions. This provides circumstantial evidence for regional-scale, fluid-flow channelling along the base of the impermeable intrusions.

Comparison to other provinces

The Diabasodden Suite is comparable to numerous igneous provinces with respect to the igneous geometries but distinguishes itself through the onshore-offshore correlation component (Table 4). It shares good onshore exposures with the well-known Karoo Basin of South Africa, but also includes a dense database, particularly offshore seismic and magnetic data. In terms of scale, the 200,000 km^2 extent estimated by Maher (2001) for the whole onshore-offshore province would make it one of the largest provinces. The 3500 km^2 study area addressed in this contribution is just a fractional subset of the Diabasodden Suite, and further focused studies are required to fully understand the igneous province.

Impact on reservoir properties

The geometry of the igneous intrusions has an impact on the reservoir properties at multiple scales. On a regional scale, reservoir compartmentalisation by extensive dykes, transgressive sills or saucer-shaped intrusions capped by a sealing shale may occur. On a smaller scale, fluid flow may be channelled along the margins of both sills and dykes, rather than flowing across them. Furthermore, the emplacement of large igneous intrusions within organic-rich source rocks of the Botneheia and Agardhfjellet formations locally probably leads to enhanced hydrocarbon generation from the thermal response to intrusive emplacement, as studied at other localities (e.g., Aarnes et al., 2010). Hubred (2006) conducted a study on the 30 m-thick Botneheia sill and concluded that commercial quantities of hydrocarbons would not be generated by a single sill. However, stacked sills and igneous centres may locally generate considerable quantities of hydrocarbons (Aarnes et al., 2011). Apart from a decreasing TOC value within the thermal aureole of the intrusion, a decrease in porosity and an increase in seismic velocity would also be expected, as shown by a study of a contact zone of an intrusion in the Karoo Basin (Haave, 2005). On the local scale, increased fracturing of host rocks during emplacement, due largely to the uplifting of the overburden by the intrusion, is evident even within and around the small-scale (2 m thin) intrusion penetrated by the Dh4 borehole in Adventdalen.

Dyke orientation and stress regime during emplacement

The orientation of igneous lineaments appears focused along two main trends: NW–SE and NE–SW (Fig. 13). Orientations derived from the lidar data illustrate a broader spread, particularly with respect to the dip angle, but in general also line up with these trends. Since dykes are typically emplaced along extensional fractures oriented perpendicular to the maximum horizontal stress, these findings may suggest NW–SE- and NE–SW-oriented maximum stress fields during the emplacement in Early

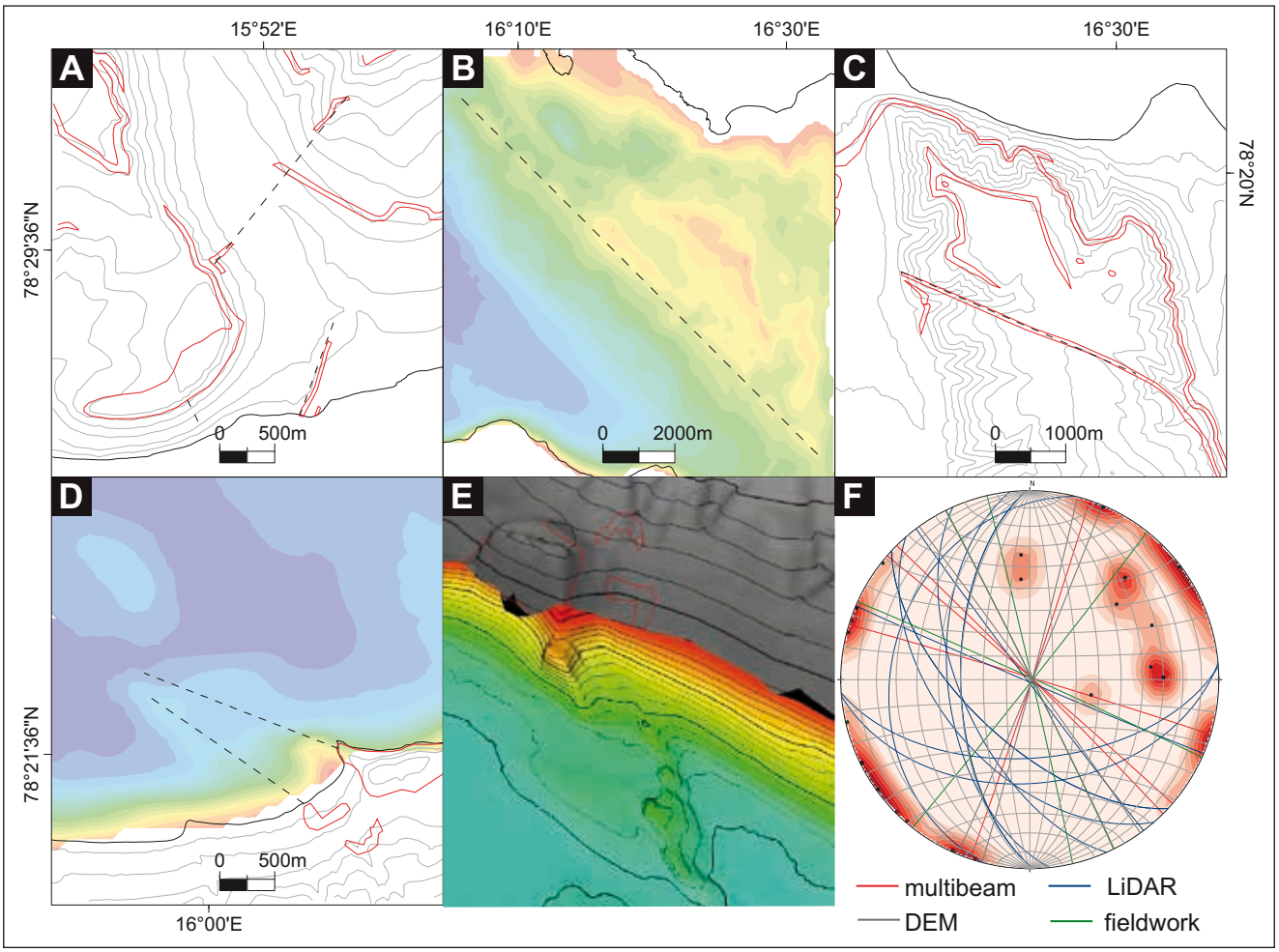

Figure 13. *Examples of onshore and offshore lineaments. Onshore these are clearly caused by dykes, and can be traced offshore in some areas. Lineaments are shown with dashed lines. (A) Three dykes exposed near the mouth of Studentdalen in southern Dickson Land. (B) Long (c. 14 km) lineament north of Diabasodden, perhaps related to a dyke. The lineament corresponds to dolerite D1 listed in Table 4. (C) Map of the Botneheia dyke and its exposure. (D) Example of onshore-offshore correlation of a dyke at Hatten. (E) 3D view of the intrusion shown in (D), illustrating the positive relief feature on the seafloor. 3x vertical exaggeration, view towards southeast. (F) Stereoplot summarising the lineament orientations analysed using different methods. Note the bipolar distribution, with dominant NW–SE and NE–SW trends.*

Cretaceous time. This agrees to an extent with N–S palaeostress measurements on Lower Cretaceous rock units in western Spitsbergen (Kleinspehn et al., 1989).

Implications for regional fluid flow and CO_2 storage

In this study, we have investigated the geometry of intrusions within an aquifer currently explored for CO_2 sequestration (Braathen et al., 2012; Ogata et al., 2012). This applied aspect focused on addressing two linked hypotheses:

1) Igneous intrusions form pressure compartments within the CO_2 storage target aquifer.
2) Igneous intrusions affect regional fluid flow in the CO_2 storage target aquifer and may lead to enhanced mobility of fluids in the subsurface.

To address these hypotheses a schematic diagram illustrating the overall geometry of the igneous system in central Spitsbergen was devised and is shown in Fig. 14. Well data show a substantial (30–60 bar), subhydrostatic, pressure regime in the target reservoir at the planned injection site in Adventdalen (Braathen et al., 2012). The gently dipping reservoir reaches the surface just 15 km from the well site, which should allow pressure communication with the surface. The observed underpressure must thus originate from local compartmentalisation caused by the presence of lateral flow barriers (e.g., faults, lateral pinch-outs, permafrost, igneous intrusions or a combination thereof; Ogata et al., 2012). The presence of saucer-shaped intrusions within the lower part of the stratigraphy may assist in creating three-dimensional compartments bounded partly by igneous intrusions and partly by sealing shales. Due to their three-dimensional geometry, saucer-shaped sills may, in conjunction with a sealing shale layer or a layer-parallel sill, compartmentalise the target aquifer. Sets of igneous dykes with a bimodal

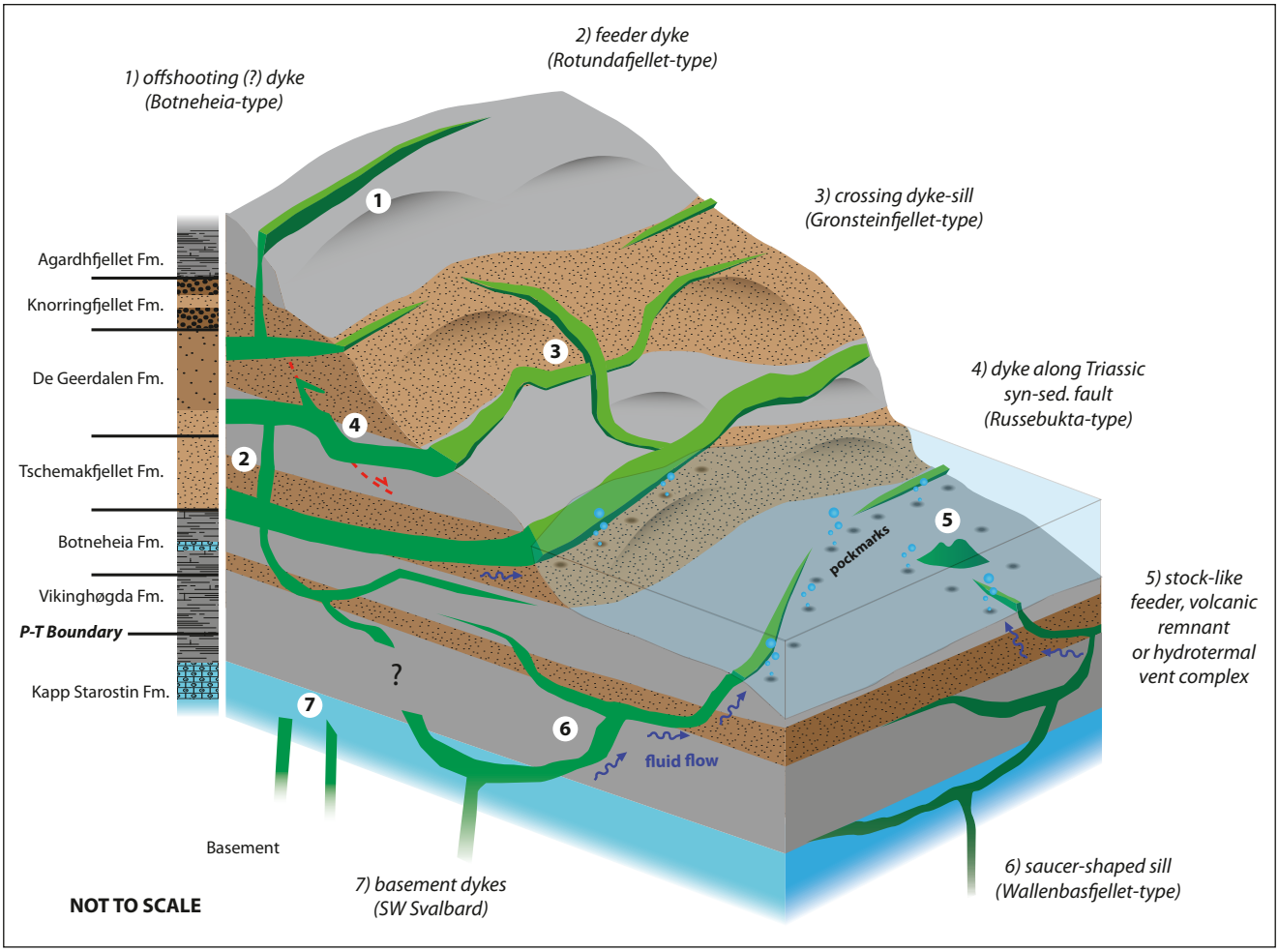

Figure 14. *Conceptual diagram summarising the prevalent geometries of igneous intrusions in central Spitsbergen. The schematic diagram illustrates the present-day situation in the study area, highlighting the different igneous geometries present. Igneous intrusions are present from the Permian Kapp Starostin Formation to the Jurassic Agardhfjellet Formation. While large-scale sills, some possibly exhibiting saucer-shaped morphologies, are present near the base of the studied stratigraphy, more complex features including dyke/sill interactions characterise the upper part. At the very top, only one dyke penetrates the Agardhfjellet Formation but, due to erosion, its upper limit cannot be defined. The conceptual figure also illustrates the possible nature of focused fluid flow along the base of the intrusions, culminating as pockmark strings on the lower edges of exposed inclined sheets.*

orientation, as illustrated in Fig. 13F, may also contribute to compartmentalising the aquifer. The lack of clear three-dimensional compartments in the study area, as well as complex geometries typically resulting in compartments being locally compromised by through-going fractures along intrusion junctions, nonetheless suggests that the intrusions are unlikely to form pressure compartments in the CO_2 target aquifer. However, the pressure regime clearly requires a lateral flow barrier and igneous intrusions may contribute locally to establishing such a barrier in conjunction with subseismic faults and stratigraphic pinch-outs. Vertical pressure compartmentalisation, as evidenced by different pressure regimes in Dh4, is likely to be a function of lithology, and particularly impermeable shale layers. However, a 2 m-thick igneous intrusion at the base of Dh4 may also contribute locally to vertical compartmentalisation, depending on its geometry.

In this study we have shown that igneous intrusions occur within the target aquifer. The orientation of dykes is both parallel and perpendicular to the presumed up-dip migration of CO_2, and may provide an additional barrier or baffle for injected CO_2. However, increased fracturing along the contact margins of sills and dykes with their host rocks also leads to locally enhanced permeability and channelling of fluid flow along the contact zones (Wilkes et al., 2004; Mège & Rango, 2010). Furthermore, the preference of sills to intrude shales and other low-permeability host rocks is likely to channel flow through otherwise sealing units, which may have consequences with respect to fluid migration into the lower part of the cap rock succession. We thus conclude that it is very likely that igneous intrusions affect the regional fluid flow and their correct representation is critical for forecasting fluid migration in the subsurface, as well as the areal extent of the CO_2 plume. The segmentation of the reservoir, as well as the enhanced contact-zone permeability, will be dependent on the scale of the intrusions. Thicker intrusions, such as the regional sills identified in De Geerdalen and on the north side of Isfjorden, are less likely to have their sealing capacity compromised by the pervasive natural fracturing in dolerites. In contrast, thin dykes and sills are likely to be cut by through-going fractures, thus providing pathways for fluid flow.

Conclusions

From the integrated study of an offshore-onshore magmatic province on Spitsbergen we infer the following:

- The prevalent geometry of the igneous system is dominated by layer-parallel sills in shale-dominated lithologies, with subordinate dykes locally present.
- Structural complexity appears to decrease with depth in the stratigraphy, reflected by increasingly complex geometries on the southern shore of Isfjorden compared with the north shore. A possible local feeder system is identified at Hatten, testified by the igneous stock with branching dykes.
- The offshore-onshore linkage of the igneous bodies is evident using magnetic, seismic, bathymetric and topographic data. Some of the NW–SE–aligned positive relief features on the seabed have been classified as dolerite ridges.
- A probable hydrothermal vent complex is interpreted south of Kapp Thordsen on the basis of a flowering structure and a magnetic low anomaly. This may have significance for atmospheric degassing following subsurface magma emplacement and associated contact metamorphism.
- The increased presence of aligned pockmarks on the seafloor provides circumstantial evidence for focused fluid channelling along the base of impermeable sills to the surface.
- A probable saucer-shaped sill has been identified in 2D seismic data covering offshore Bjørndalen, approximately 20 km from a planned CO_2 injection site.
- Based on the present dataset, it is unlikely that igneous intrusions alone can create sealing pressure compartments within the CO_2 target aquifer. However, in conjunction with stratigraphic pinch-outs and faults they can contribute to the reservoir segmenting, which is necessary in order to generate the current subhydrostatic pressure regime.
- Fluids are likely to be both channelled and baffled by the igneous intrusions, particularly by dykes. Depending on their orientation and prevalent fluid flow the intrusions will thus exert some control on the areal extent of a potential CO_2 plume.
- The study can be used as a solid input base for establishing a regional reservoir model both for CO_2 injection and for understanding natural fluid flow in the study area.

Acknowledgements. This work was financed by the Norwegian Research Council ('GeC' project in the CLIMIT program), in collaboration with the UNIS CO_2 lab (http://co2-ccs.unis.no). The first author's fieldwork was financed by Arctic Field Grants from the Svalbard Science Forum. The multibeam bathymetric data from the Norwegian Hydrographic Service was presented in accordance with permission number 13/G706. The Norwegian Polar Institute provided the shape files of the geological maps (NPI–Geonet project) and aerial photographs. Schlumberger provided an academic license of Petrel. Svalex, a Statoil-sponsored educational project, generously provided access to 2D seismic and magnetic data. Base station magnetic data were provided by Truls Lynne Hansen at the Tromsø Geophysical Observatory. OpenStereo (Grohmann & Campanha, 2010) was used for plotting stereoplots. Ingrid Anell reviewed an earlier version of this manuscript. A special thank you goes to our field assistants Andreas Rittersbacher, Dave Richey, Lilith Kuckero, Marie Marušková and Sabine Rumpf. Finally, we sincerely appreciate the constructive comments by the reviewers Dougal Jerram and Sergio Rocchi, and the editor Trond Slagstad.

References

Aarnes, I., Svensen, H., Connolly, J.A.D. & Podladchikov, Y.Y. 2010: How contact metamorphism can trigger global climate changes:

Modeling gas generation around igneous sills in sedimentary basins. *Geochimica et Cosmochimica Acta 74*, 7179–7195.

Aarnes, I., Svensen, H., Polteau, S. & Planke, S. 2011: Contact metamorphic devolatilization of shales in the Karoo Basin, South Africa, and the effects of multiple sill intrusions. *Chemical Geology 281*, 181–194.

Airoldi, G., Muirhead, J.D., Zanella, E. & White, J.D.L. 2012: Emplacement process of Ferrar Dolerite sheets at Allan Hills (South Victoria Land, Antarctica) inferred from magnetic fabric. *Geophysical Journal International 188*, 1046–1060.

Amundsen, H., Evokimov, A., Dibner, V.D. & Andresen, A. 1998: Geochemistry and petrogenetic significance of mesozoic magmatism on Franz Josef Land, northeastern Barents Sea. *In* Solheim, A., Musatov, E. & Heintz, N. (eds.): *Geological Aspects of Franz Joseph Land and the northernmost Barents Sea*, Norsk Polarinstitutt Meddelelser Nr. 151. Oslo, Norsk Polarinstitutt, pp. 105–120.

Asghar, A. 2011: *Processing and Interpretation of Multichannel Seismic Data from Isfjorden, Svalbard*. MSc thesis, University of Bergen, 123 pp.

Baeten, N.J., Forwick, M., Vogt, C. & Vorren, T.O. 2010: Late Weichselian and Holocene sedimentary environments and glacial activity in Billefjorden, Svalbard. *In* Howe, J. A., Austin, W.E.N., Forwick, M. & Paetzel, M. (eds.): *Fjord Systems and Archives. London*, Geological Society, pp. 207–223.

Bergh, S.G., Braathen, A. & Andresen, A. 1997: Interaction of basement-involved and thin-skinned tectonism in the Tertiary fold-thrust belt of central Spitsbergen, Svalbard. *American Association of Petroleum Geologists Bulletin 81*, 637–661.

Birkenmajer, K. & Morawski, T. 1960: Dolerite intrusions of Wedel-Jarlsberg Land, Vestspitsbergen. *Studia Geologica Polonica IV*, 103–123.

Birkenmajer, K., Krajewski, K.P., Pécskay, Z. & Lorenc, M.W. 2010: K–Ar dating of basic intrusions at Bellsund, Spitsbergen, Svalbard. *Polish Polar Research 31*, 3–16.

Blinova, M., Faleide, J.I., Gabrielsen, R.H. & Mjelde, R. 2012: Seafloor expression and shallow structure of a fold-and-thrust system, Isfjorden, west Spitsbergen. *Polar Research 31*, 11209, http://dx.doi.org/10.3402/polar.v31i0.11209.

Blomeier, D., Dustira, A., Forke, H. & Scheibner, C. 2011: Environmental change in the Early Permian of NE Svalbard: from a warm-water carbonate platform (Gipshuken Formation) to a temperate, mixed siliciclastic-carbonate ramp (Kapp Starostin Formation). *Facies 57*, 493–523.

Braathen, A., Baelum, K., Christiansen, H.H., Dahl, T., Eiken, O., Elvebakk, H., Hansen, F., Hanssen, T.H., Jochmann, M., Johansen, T.A., Johnsen, H., Larsen, L., Lie, T., Mertes, J., Mørk, A., Mørk, M.B., Nemec, W.J., Olaussen, S., Oye, V., Rød, K., Titlestad, G.O., Tveranger, J. & Vagle, K. 2012: Longyearbyen CO_2 lab of Svalbard, Norway – first assessment of the sedimentary succession for CO_2 storage. *Norwegian Journal of Geology 92,* 353–376.

Buckley, S.J., Vallet, J., Braathen, A. & Wheeler, W. 2008: Oblique helicopter-based laser scanning for digital terrain modelling and visualisation of geological outcrops. *International Archives of the Photogrammetry, Remote Sensing and Spatial Information Sciences 37*, 493–498.

Burov, P., Krasil'scikov, A.A., Firsov, L.V. & Klubov, B.A. 1977: The age of Spitsbergen Dolerites (from isotopic dating). *Norsk polarinstitutt Årbok 1975*, 101–108.

Bælum, K. & Braathen, A. 2012: Along-strike changes in fault array and rift basin geometry of the Carboniferous Billefjorden Trough, Svalbard, Norway. *Tectonophysics 546–547*, 38–55.

Bælum, K., Johansen, T.A., Johnsen, H., Rød, K., Ruud, B.O. & Braathen, A. 2012: Subsurface geometries of the Longyearbyen CO_2 lab in Central Spitsbergen, as mapped by reflection seismic data. *Norwegian Journal of Geology 92*, 377–389.

Cartwright, J. & Møller Hansen, D. 2006: Magma transport through the crust via interconnected sill complexes. *Geology 34*, 929–932.

Chandra, S., Rao, V., Krishnamurthy, N., Dutta, S. & Ahmed, S. 2006: Integrated studies for characterization of lineaments used to locate groundwater potential zones in a hard rock region of Karnataka, India. *Hydrogeology Journal 14*, 1042–1051.

Chevallier, L. & Woodford, A. 1999: Morpho-tectonics and mechanism of emplacement of the dolerite rings and sills of the western Karoo, South Africa. *South African Journal of Geology 102*, 43–54.

Chevallier, L., Gibson, L.A., Nhleko, L.O., Woodford, A.C., Nomquphu, W. & Kippie, I. 2004: Hydrogeology of fractured-rock aquifers and related ecosystems within the Qoqodala dolerite ring and sill complex, Great Kei catchment, Eastern Cape. *Water Resource Commission Reports, WRC Report No. 1238/1/04*, 150 pp.

Corfu, F., Polteau, S., Planke, S., Faleide, J.I., Svensen, H., Zayoncheck, A. & Stolbov, N. 2013: U–Pb geochronology of Cretaceous magmatism on Svalbard and Franz Josef Land, Barents Sea Large Igneous Province. *Geological Magazine 150*, 1127–1135.

Cukur, D., Horozal, S., Kim, D., Lee, G., Han, H. & Kang, M. 2010: The distribution and characteristics of the igneous complexes in the northern East China Sea Shelf Basin and their implications for hydrocarbon potential. *Marine Geophysical Research 31*, 299–313.

Dallmann, W.K., Dypvik, H., Gjelberg, J.G., Harland, W.B., Johannessen, E.P., Keilen, H.B., Larssen, G.B., Lønøy, A., Midbøe, P.S., Mørk, A., Nagy, J., Nilsson, I., Nøttvedt, A., Olaussen, S., Pcelina, T.M., Steel, R.J. & Worsley, D. 1999: *Lithostratigraphic Lexicon of Svalbard: Review and recommendations for nomenclature use*, Tromsø, Norsk Polarinstitutt, 318 pp.

Digranes, P. & Kristoffersen, Y. 1995: Use of mode-converted waves in marine seismic data to investigate the lithology of the sub-bottom sediments in Isfjorden, Svalbard. *Pure and Applied Geophysics 145*, 313–325.

Dimakis, P., Braathen, B.I., Faleide, J.I., Elverhøi, A. & Gudlaugsson, S.T. 1998: Cenozoic erosion and the preglacial uplift of the Svalbard–Barents Sea region. *Tectonophysics 300*, 311–327.

Dörr, N., Lisker, F., Clift, P.D., Carter, A., Gee, D.G., Tebenkov, A.M. & Spiegel, C. 2012: Late Mesozoic–Cenozoic exhumation history of northern Svalbard and its regional significance: Constraints from apatite fission track analysis. *Tectonophysics 514–517*, 81–92.

Eiken, O. 1994: Seismic atlas of Western Svalbard : a selection of regional seismic transects. *Norsk Polarinstitutt Meddelelser, 130*, 1–73.

Elvevold, S., Dallmann, W. & Blomeier, D. (eds.) 2007: *Geology of Svalbard*. Tromsø, Norwegian Polar Institute, 38.

Ferraccioli, F., Gambetta, M. & Bozzo, E. 1998: Microlevelling procedures applied to regional aeromagnetic data: an example from the Transantarctic Mountains (Antarctica). *Geophysical Prospecting 46*, 177–196.

Galerne, C.Y., Neumann, E.R. & Planke, S. 2008: Emplacement mechanisms of sill complexes: Information from the geochemical architecture of the Golden Valley Sill Complex, South Africa. *Journal of Volcanology and Geothermal Research 177*, 425–440.

Gallagher, J.W. & Dromgoole, P.W. 2008: Seeing below the basalt – offshore Faroes. *Geophysical Prospecting, 56*, 33–45.

Geosoft 2005: Montaj Geophysics Levelling System, processing and enhancing geophysical data extension for Oasis Montaj v.6.2 (Tutorial and user guide). Geosoft Incorporated, 68 pp.

Grohmann, C.H. & Campanha, G.A. 2010: OpenStereo: Open Source, Cross-Platform Software for Structural Geology Analysis (http://www.igc.usp.br/index.php?id=openstereo). *AGU Fall Meeting, 13–17 December 2010*. San Francisco, USA.

Grove, C. 2013: Submarine hydrothermal vent complexes in the Paleocene of the Faroe–Shetland Basin: Insights from three-dimensional seismic and petrographical data. *Geology, 41*, 71–74.

Gudmundsson, A. & Løtveit, I.F. 2012: Sills as fractured hydrocarbon reservoirs: examples and models. *In* Spence, G.H., Redfern, J., Aguilera, R., Bevan, T.G., Cosgrove, J.W., Couples, G.D. & Daniel, J.M. (eds.): *Advances in the Study of Fractured Reservoirs*, *Geological Society of London Special Publication 374*, doi:10.1144/SP374.5.

Haave, C. 2005: *Metamorphic and petrophysical effects of sill intrusions in sedimentary strata: the Karoo Basin, South Africa*. MSc thesis, University of Oslo, 168 pp.

Hansen, D.M. & Cartwright, J. 2006: The three-dimensional geometry

and growth of forced folds above saucer-shaped igneous sills. *Journal of Structural Geology 28*, 1520–1535.

Hansen, D.M., Redfern, J., Federici, F., di Biase, D. & Bertozzi, G. 2008: Miocene igneous activity in the Northern Subbasin, offshore Senegal, NW Africa. *Marine and Petroleum Geology 25*, 1–15.

Hansen, J., Jerram, D.A., McCaffrey, K. & Passey, S.R. 2009: The onset of the North Atlantic Igneous Province in a rifting perspective. *Geological Magazine 146*, 309–325.

Hansen, J., Jerram, D.A., McCaffrey, K. & Passey, S.R. 2011: Early Cenozoic saucer-shaped sills of the Faroe Islands: an example of intrusive styles in basaltic lava piles. *Journal of the Geological Society 168*, 159–178.

Haremo, P., Andresen, A. & Dypvik, H. 1993: Mesozoic extension versus Tertiary compression along the Billefjorden Fault Zone south of Isfjorden, central Spitsbergen. *Geological Magazine 130*, 783–795.

Harland, W.B. 1997: *The Geology of Svalbard*. Geological Society Memoir 17, The Geological Society, Bath, United Kingdom, 525 pp.

Helland-Hansen, W. 2010: Facies and stacking patterns of shelf-deltas within the Palaeogene Battfjellet Formation, Nordenskiöld Land, Svalbard: implications for subsurface reservoir prediction. *Sedimentology 57*, 190–208.

Hubred, J.H. 2006: *Thermal Effects of Basaltic Sill Emplacement in Source Rocks on Maturation and Hydrocarbon Generation*. MSc thesis, University of Oslo, 303 pp.

Høy, T. & Lundschien, B.A. 2011: Triassic deltaic sequences in the northern Barents Sea. *In* Spencer, A.M., Embry, A.F., Gautier, D.L., Stoupakova, A.V. & Sørensen, K. (eds.): *Arctic Petroleum Geology, Geological Society of London Memoir 35*, pp. 249–260.

Jackson, K.C. & Halls, H.C. 1988: Tectonic implications of paleomagnetic data from sills and dykes in the Sverdrup Basin, Canadian Arctic. *Tectonics 7*, 463–481.

Jamtveit, B., Svensen, H., Podladchikov, Y.Y. & Planke, S. 2004: Hydrothermal vent complexes associated with sill intrusions in sedimentary basins. *In* Breitkreuz, C. & Petford, N. (eds.): *Physical Geology of High-Level Magmatic Systems*, Geological Society of London Special Publication 234, 233–241.

Jeleńska, M., Kądziałko-Hofmokl, M., Kruczyk, J. & Vincenz, S.A. 1978: Thermomagnetic properties of some Late Mesozoic diabase dikes of South Spitsbergen. *Pure and Applied Geophysics 117*, 784–794.

Johannessen, E.P. & Steel, R.J. 1992: Mid-Carboniferous extension and rift-infill sequences in the Billefjorden Trough, Svalbard. *Norsk geologisk tidsskrift 72*, 35–48.

Johansen, T.A., Digranes, P., van Schaack, M. & Lønne, I. 2003: Seismic mapping and modeling of near-surface sediments in polar areas. *Geophysics 68*, 566–573.

Joppen, M. & White, R.S. 1990: The Structure and Subsidence of Rockall Trough From Two-Ship Seismic Experiments. *Journal of Geophysical Research 95*, 19821–19837.

Kleinspehn, K.L., Pershing, J. & Teyssier, C. 1989: Paleostress stratigraphy: A new technique for analyzing tectonic control on sedimentary-basin subsidence. *Geology 17*, 253–256.

Lee, G.H., Kwon, Y.I., Yoon, C.S., Kim, H.J. & Yoo, H.S. 2006: Igneous complexes in the eastern Northern South Yellow Sea Basin and their implications for hydrocarbon systems. *Marine and Petroleum Geology 23*, 631–645.

Luyendyk, A. 1997: Processing of airborne magnetic data. Australian Geological Survey Organisation, *Journal of Australian Geology and Geophysics 17*, 31–38.

Maher, H.D. Jr. 2001: Manifestations of the Cretaceous High Arctic Large Igneous Province in Svalbard. *The Journal of Geology 109*, 91–104.

Mauring, E., Beard, L.P., Kihle, O. & Smethurst, M.A. 2002: A comparison of aeromagnetic levelling techniques with an introduction to median levelling. *Geophysical Prospecting 50*, 43–54.

Mège, D. & Rango, T. 2010: Permanent groundwater storage in basaltic dyke fractures and termite mound viability. *Journal of African Earth Sciences 57*, 127–142.

Meyer, R., van Wijk, J. & Gernigon, L. 2007: The North Atlantic Igneous Province: A review of models for its formation. *Geological Society of America Special Papers 430*, 525–552.

Miles, A. & Cartwright, J. 2010: Hybrid flow sills: A new mode of igneous sheet intrusion. *Geology 38*, 343–346.

Milovslavskij, M.J., Birjukov, A.S., Slenskij, S.N., Hansen, S., Larsen, B.T., Dallmann, W. K., Andresen, A., Dypvik, H., Krasilscikov, A.A., Birkeland, Ø. & Salvigsen, O. 1993: Geological Map of Svalbard: 1:000,000, Sheet D9G Agardhfjellet (with accompanying text). *Norsk Polarinstitutt Temakart 21*, 42 pp.

Minakov, A., Mjelde, R., Faleide, J.I., Flueh, E.R., Dannowski, A. & Keers, H. 2012: Mafic intrusions east of Svalbard imaged by active-source seismic tomography. *Tectonophysics 518–521*, 106–118.

Morel, E.H. & Wikramaratna, R.S. 1982: Numerical modelling of groundwater flow in regional aquifers dissected by dykes. *Hydrological Sciences Journal 27*, 63–77.

Muirhead, J.D., Airoldi, G., Rowland, J.V. & White, J.D.L. 2012: Interconnected sills and inclined sheet intrusions control shallow magma transport in the Ferrar large igneous province, Antarctica. *Geological Society of America Bulletin 124*, 162–180.

Mørk, A., Knarud, R. & Worsley, D. 1982: Depositional and diagenetic environments of the Triassic and Lower Jurassic succession of Svalbard. *In* Embry, A.F. & Balkwill, H.R. (eds.): *Arctic Geology and Geophysics*, Canadian Society of Petroleum Geologists Memoir 8, pp. 371–398.

Nejbert, K., Krajewski, K.P., Dubińska, E. & Pécskay, Z. 2011: Dolerites of Svalbard, north-west Barents Sea Shelf: age, tectonic setting and significance for geotectonic interpretation of the High-Arctic Large Igneous Province. *Polar Research 30*, 1–24.

NPI 2011: NPI–Geonet Project, accessed 10/12/2012. *http://geonet.npolar.no/items-general/frame.html*.

Nøttvedt, A., Livbjerg, F., Midbøe, P.S. & Rasmussen, E. 1993: Hydrocarbon potential of the Central Spitsbergen Basin. *In* Vorren, T.O., Bergsager, E., Dahl-Stamnes, Ø.A., Holter, E., Johansen, B., Lie, E. & Lund, T.B. (eds.): *Arctic Geology and Petroleum Potential*. Amsterdam, Elsevier, pp. 333–361.

Ogata, K., Senger, K., Braathen, A., Tveranger, J. & Olaussen, S. 2012: The importance of natural fractures in a tight reservoir for potential CO_2 storage: case study of the upper Triassic to middle Jurassic Kapp Toscana Group (Spitsbergen, Arctic Norway). *In* Spence, G.H., Redfern, J., Aguilera, R., Bevan, T.G., Cosgrove, J.W., Couples, G.D. & Daniel, J.M. (eds.): *Advances in the Study of Fractured Reservoirs*, Geological Society of London Special Publication 374, doi:10.1144/SP374.9.

Perrin, J., Ahmed, S. & Hunkeler, D. 2011: The effects of geological heterogeneities and piezometric fluctuations on groundwater flow and chemistry in a hard-rock aquifer, southern India. *Hydrogeology Journal 19*, 1189–1201.

Planke, S., Rasmussen, T., Rey, S.S. & Myklebust, R. 2005: Seismic characteristics and distribution of volcanic intrusions and hydrothermal vent complexes in the Vøring and Møre basins. *In* Dore, A.G. & Vinning, B.A. (eds.): *Proceedings of the 6th Petroleum Geology Conference. London*, Geological Society, pp. 833–844.

Polteau, S., Mazzini, A., Galland, O., Planke, S. & Malthe-Sørenssen, A. 2008: Saucer-shaped intrusions: Occurrences, emplacement and implications. *Earth and Planetary Science Letters 266*, 195–204.

Polteau, S., Planke, S., Planke, E.E., Faleide, J.I., Svensen, H., Corfu, F., Midtkandal, I. & Myklebust, R. 2011: The Barents Sea Large Igneous Province: Extent, Age & Global Implications. *Norwegian Geological Society Winter Meeting, 11–13 January 2011*. Stavanger, Norway.

Rateau, R., Schofield, N. & Smith, M. 2013: The potential role of igneous intrusions on hydrocarbon migration, West of Shetland. *Petroleum Geoscience 19*, 259-272.

Rittersbacher, A., Buckley, S.J., Howell, J.A., Hampson, G.J. & Vallet, J. 2013: Helicopter-based laser scanning: a method for quantitative analysis of large-scale sedimentary architecture. *In* Martinius, A.W., Howell, J.A. & Good, T. (eds.): Sediment-body Geometry

and Heterogeneity: Analogue Studies for Modelling the Subsurface, Geological Society of London Special Publication 387, pp. 1–18.

Roberts, A.W., White, R.S. & Christie, P.A.F. 2009: Imaging igneous rocks on the North Atlantic rifted continental margin. *Geophysical Journal International 179*, 1024–1038.

Rocchi, S., Mazzotti, A., Marroni, M., Pandolfi, L., Costantini, P., Giuseppe, B., Biase, D. d., Federici, F. & Lô, P. G. 2007: Detection of Miocene saucer-shaped sills (offshore Senegal) via integrated interpretation of seismic, magnetic and gravity data. *Terra Nova 19*, 232–239.

Roy, S., Senger, K., Noormets, R. & Hovland, M. 2012: Pockmarks in the fjords of western Svalbard and their implications on gas hydrate dissociation. *Geophysical Research Abstracts 14*, EGU2012–8960.

Rygg, E., Riste, P., Nøttvedt, A., Rød, K. & Kristoffersen, Y. 1993: The Snowstreamer – a new device for acquisition of seismic data on land. *In* Vorren, T.O., Bergsager, E., Dahl-Stamnes, Ø.A., Holter, E., Johansen, B., Lie, E. & Lund, T.B. (eds.): *Arctic Geology and Petroleum Potential*. Amsterdam, Elsevier, pp. 703–709.

Schlumberger 2011: Petrel E&P Software Platform, v. 2011. Software.

Schofield, N., Heaton, L., Holford, S.P., Archer, S.G., Jackson, C.A.-L. & Jolley, D.W. 2012: Seismic imaging of 'broken bridges': linking seismic to outcrop-scale investigations of intrusive magma lobes. *Journal of the Geological Society 169*, 421–426.

Shipilov, E. & Karyakin, Y. 2010: New data on basaltoid magmatism of western Spitsbergen. *Doklady Earth Sciences 430*, 252–257.

Silantyev, S.A., Bogdanovskii, O.G., Fedorov, P.I., Karpenko, S.F. & Kostitsyn, Y.A. 2004: Intraplate magmatism of the De Long Islands: A response to the propagation of the ultraslow-spreading Gakkel Ridge into the passive continental margin in the Laptev Sea. *Russian Journal of Earth Sciences 6*, 153–183.

Skola, I.V., Pcelina, T.M., Mazur, V.B. & Alter, S.M. 1980: New data on the composition and structure of the sedimentary platform cover on the basis of materials from the drilling of a parametric hole at Grumantbyen. *Geology of the sedimentary platform cover of the archipelago of Svalbard. Collection of scientific papers*. Leningrad, NIIGA, pp. 13–24.

Smallwood, J.R. & Maresh, J. 2002: The properties, morphology and distribution of igneous sills: modelling, borehole data and 3D seismic from the Faroe–Shetland area. *In* Jolley, D.W. & Bell, B.R. (eds.): *The North Atlantic Igneous Province: Stratigraphy, Tectonic, Volcanic and Magmatic Processes*, Geological Soceity of London Special Publication 197, pp. 271–306.

Smith, D.G., Harland, W.B., Hughes, N.F. & Pickton, C.A.G. 1976: The geology of Kong Karls Land, Svalbard. *Geological Magazine 113*, 193–232.

Steel, R.J. & Worsley, D. 1984: Svalbard's post-Caledonian strata – an atlas of sedimentational patterns and paleogeographic evolution. *In* Spencer, A.M. (ed.): *Petroleum Geology of the North European Margin*. Graham & Trotman, London, pp. 109–135.

Svensen, H., Planke, S., Malthe-Sorenssen, A., Jamtveit, B., Myklebust, R., Rasmussen Eidem, T. & Rey, S.S. 2004: Release of methane from a volcanic basin as a mechanism for initial Eocene global warming. *Nature 429*, 542–545.

Svensen, H., Jamtveit, B., Planke, S. & Chevallier, L. 2006: Structure and evolution of hydrothermal vent complexes in the Karoo Basin, South Africa. *Journal of the Geological Society 163*, 671–682.

Svensen, H., Corfu, F., Polteau, S., Hammer, Ø. & Planke, S. 2012: Rapid magma emplacement in the Karoo Large Igneous Province. *Earth and Planetary Science Letters 325–326*, 1–9.

Tegner, C., Storey, M., Holm, P.M., Thorarinsson, S.B., Zhao, X., Lo, C.H. & Knudsen, M.F. 2011: Magmatism and Eurekan deformation in the High Arctic Large Igneous Province: ^{40}Ar–^{39}Ar age of Kap Washington Group volcanics, North Greenland. *Earth and Planetary Science Letters 303*, 203–214.

Thomson, K. 2004: Sill complex geometry and internal architecture: a 3D seismic perspective. *In* Breitkreuz, C. & Petford, N. (eds.): *Physical Geology of High-Level Magmatic Systems*, Geological Society of London Special Publication 234, pp. 229–232.

Thomson, K. & Hutton, D. 2004: Geometry and growth of sill complexes: insights using 3D seismic from the North Rockall Trough. *Bulletin of Volcanology 66*, 364–375.

Throndsen, T. 1982: Vitrinite reflectance studies of coals and dispersed organic matter in Tertiary deposits in the Adventdalen area, Svalbard. *Polar Research 2*, 77–91.

Tyrrell, G.W. & Sandford, K.S. 1933: Geology and petrology of dolerites of Spitsbergen. *Proceedings of the Royal Society of Edinburgh 53*, 284–341.

Vincenz, S.A. & Jeleńska, M. 1985: Paleomagnetic investigations of Mesozoic and Paleozoic rocks from Svalbard. *Tectonophysics 114*, 163–180.

Wennberg, O.P., Andresen, A., Hansen, S. & Bergh, S.G. 1994: Structural evolution of a frontal ramp section of the West Spitsbergen, Tertiary fold and thrust belt, north of Isfjorden, Spitsbergen. *Geological Magazine 131*, 67–80.

Wetmore, P.H., Connor, C.B., Kruse, S.E., Callihan, S., Pignotta, G., Stremtan, C. & Burke, A. 2009: Geometry of the Trachyte Mesa intrusion, Henry Mountains, Utah: Implications for the emplacement of small melt volumes into the upper crust. *Geochemistry Geophysics Geosystems 10*, Q08006, doi:10.1029/2009GC002469.

Wilkes, S.M., Clement, T.P. & Otto, C.J. 2004: Characterisation of the hydrogeology of the Augustus River catchment, Western Australia. *Hydrogeology Journal 12*, 209–223.

Witte, J., Bonora, M., Carbone, C. & Oncken, O. 2012: Fracture evolution in oil-producing sills of the Rio Grande Valley, northern Neuquén Basin, Argentina. American Association of Petroleum *Geologists Bulletin 96*, 1253–1277.

Worsley, D. 2008: The post-Caledonian development of Svalbard and the western Barents Sea. *Polar Research 27*, 298–317.